Electrochemical and Spectroelectrochemical Studies of Porphyrazines and Related Precursors

---

A Thesis

Presented to

the Faculty of the Department of Chemistry

University of Houston

In Partial Fulfillment

of the Requirements for the

Masters of Science

---

by

David H. Futur

December 2013

Electrochemical and Spectroelectrochemical Studies of Porphyrazines and Related Precursors

_____

David H. Futur

Approved:

_____

Dr. Karl M. Kadish, Chairman

_____

Dr. Steven Baldelli

_____

Dr. Eric Van Caemelbecke

_____

Dr. Randolph Thummel

_____

Dr. Ding-Shyue Yang

_____

Dean, College of Natural Sciences and Mathematics

Dedication

This dissertation is dedicated to

my parents, Haile Futur and Frewoini Zeketar,

and my sister, Rahya Futur.

Acknowledgments

I would to express my appreciation to Dr. Karl M. Kadish for giving me the opportunity to learn from and work with him.

I also want to acknowledge Dr. Claudio Ercolani and Dr. Maria Pia Donzello for supplying the compounds analyzed in this thesis.

Finally, I want to express my gratitude to Dr. Siyabonga Ngnubane, Dr. Zhen Fu, and my cousin, Aron Araya, whose support and advice were invaluable during my time at the University of Houston.

Electrochemical and Spectroelectrochemical Studies of Porphyrazines and Related Precursors

---

An Abstract of a Thesis

Presented to

the Faculty of the Department of Chemistry

University of Houston

In Partial Fulfillment

of the Requirements for the

Masters of Science

---

by

David H. Futur

December 2013

Abstract

This thesis presents UV-visible, electrochemical, and spectroelectrochemical studies carried out in non-aqueous media of homo/heterobimetallic pyrazinoporphyrazine compounds, i.e.[($M'Cl_2$)LM] and [($PtCl_2$)(CH_3)$_6$LM](I)$_6$, where L =tetrakis-2,3-[5,6-di(2-pyridyl)pyrazino]porphyrazinato anion,M =Zn^{II}, Mg^{II}(H_2O) or Pd^{II} and M′ =Pd^{II} or Pt^{II}, 2,3-di(2-pyridyl)-6,7-dicyano-1,4-quinoxaline, [$(CN)_2Py_2Quin$], its complexes [$(CN)_2Py_2QuinMCl_2$] (M = Pd^{II}, Pt^{II}) and related pyrazine derivatives.

The [($M'Cl_2$)LM] compounds, as obtained from the mononuclear species [LM], undergo only subtle UV-visible spectral changes and exhibit practically unchanged half-wave potentials for reduction; thus, peripheral coordination to the [LM] macrocycles of a single $PdCl_2$ or $PtCl_2$ unit at one of the external dipyridinopyrazine fragments only minimally disturbs the s/pelectronic distribution within the entire porphyrazine unit. In contrast, quaternization by CH_3I of the six unligated pyridine N atoms of the species [($PtCl_2$)LM] leading to formation of the hexacations [($PtCl_2$)(CH_3)$_6$LM]$^{6+}$results in a significant bathochromic shift (5–15 nm) of the Q-band positions, thus suggesting an enhanced electron-withdrawing effect determined by an incremented displacement of the s/pelectronic system towards the periphery of the macrocycle. Accordingly, there is a facilitated thermodynamic uptake of electrons upon going from [($PtCl_2$)(CH_3)$_6$LM]$^{6+}$ to [($PtCl_2$)(CH_3)$_6$LM]n(n =5+ →2+). Noteworthy, the UV-visible spectra of the salt-like species [($PtCl_2$)(CH_3)$_6$LM](I)$_6$in water at c =5 ×10^{-5}M) indicate the presence of a monomer-dimer equilibrium, persistent even at very low concentrations (ca. 5 ×10^{-7}M).

The newly examined triad of neutral quinoxaline compounds and their corresponding pyrazine counterparts, demonstrated that the one-electron reduction of

these compounds in nonaqueous solvents generally resulted in a bathochromic shift of bands in the 250-400 nm region of the spectrum, accompanied by the formation of intense additional absorptions in the region of 500-900 nm. These spectral bands of the monoanions are theoretically examined in the present study by TDDFT calculations and interpreted in terms of single electron excitations between the Kohn-Sham orbitals of the gas-phase optimized structures.

Table of Contents

List of Abbreviations

Abbreviation	Meaning
Abs	absorbance
AN	Acetonitrile
Ar	aromatic
cpd	compound
CV	cyclic voltammetry
DMSO	dimethylsulfoxide
$E_{1/2}$	half-wave potential (in volts)
E_p	peak potential (by cyclic voltammetry)
E_{pa}	anodic peak potential (by cyclic voltammetry)
E_{pc}	cathodic peak potential (by cyclic voltammetry)
ε	molar absorptivity
Fc	ferrocene
Fc^+	ferricinium ion
H_2P	free-base porphyrin

HOMO	highest occupied molecular orbital
LUMO	lowest unoccupied molecular orbital
λ_{max}	wavelength at a specific selected peak maximum
P	porphyrin
Pc	phthalocyanine
Pyz	pyrazine
Pz	porphyrazine
Ph	phenyl
PhCN	benzonitrile
py	pyridine
Quin	quinoxaline
SCE	saturated calomel electrode
SOMO	singly occupied molecular orbital
TBACl	tetra-*n*-butylammonium chloride
TBAOH	tetra-*n*-butylammonium hydroxide
TBAP	tetra-*n*-butylammonium perchlorate

Th	thienyl
$TBAPF_6$	tetra-*n*-butylammonium hexafluorophosphate
TPP	5, 10, 15, 20-tetraphenylporphyrin dianion
OEP	1, 3, 7, 8, 12, 13, 17, 18-octaethylporphyrin dianion

List of Figures

List of Tables

CHAPTER ONE

Introduction

1.1 Porphyrazines and other Tetrapyrrolic Macrocycles

Metalloporphyrins (MP) and metalloporphyrazines (MPz) are related tetrapyrrolic macrocycles, having the core structures given in Figure 1.1. Porphyrins are made up of four pyrrole groups linked by methine bridges to form a 16 atom, 18-π-electron conjugated macrocycle. The free-base porphyrin, represented as H_2P, has a -2 charge on the deprotonated macrocycle and the two protons bound to the four central nitrogens can be replaced by metal ions having a +2, +3, +4, +5, or +6 charge.[1] In the case of M(II) ions, the metalloporphyrin is neutral while porphyrins with M(III) or M(IV) ions have axially bound anions such as in $M^{III}PX$ or $M^{IV}PX_2$, where X is usually a halide.[1]

The core of a porphyrin can be substituted at 12 different positions, four of which are at the meso carbons labeled as 5, 10, 15, and 20 in Figure 1.1, and eight are at the β-pyrrole positions labeled as 2, 3, 7, 8, 12, 13, 17, and 18 to give, for example, 5,10,15,20-tetraphenylporphyrinZn(II) (TPPZn) or 2,3,7,8,12,13,17,18-octaethylporphyrin.[1]

Metalloporphyrazines and metalloporphyrins have the same number of π-electrons in the conjugated system but the carbons bridges at the 5, 10, 15, and 20 positions of the porphyrin have been replaced by nitrogen atoms in the case of MPz (see Figure 1.1). MPz and MP are isoelectric with each other but it is important to note that the aza bridges in MPz complexes are more electronegative than the methine bridges of MP, which makes them consistently easier to reduce and harder to oxidize than MP analogues with the same metal ion.[2, 3] Phthalocyanines are the most common class of porphyrazines in which the conjugated system is expanded by the addition of a fused benzene ring to each pyrrole unit (see Figure 1.1). Porphyrazines and phthalocyanines

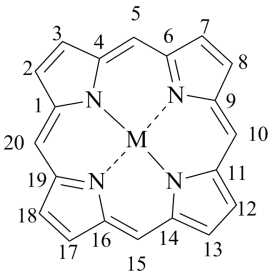

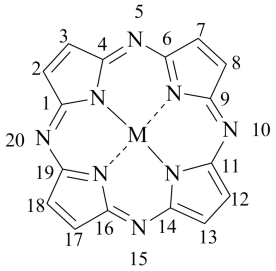

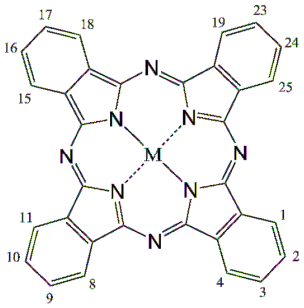

metalloporphyrin (MP) metalloporphyrazine (MPz) metallophthalocyanine (MPc)

Figure 1.1: Core structures of three related tetrapyrrole macrocycles.

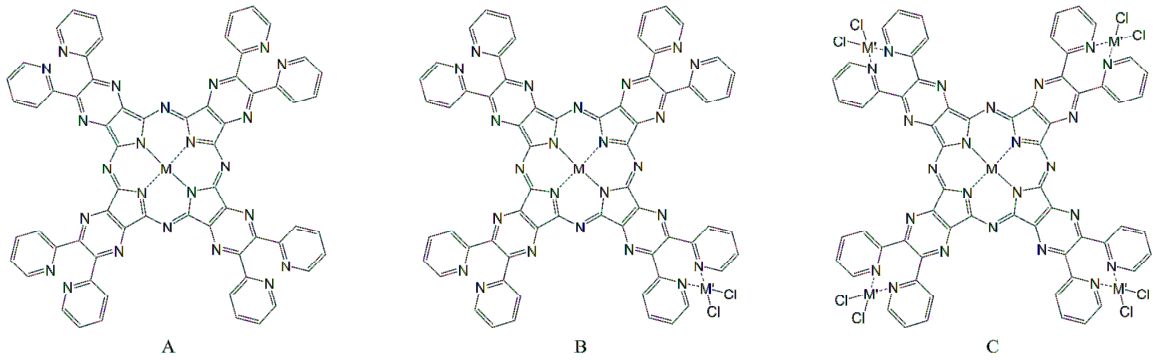

Figure 1.2. Schematic representations of A) [LM], B) [(M'Cl_2)LM], and C) [(M'Cl_2)$_4$LM], where M = $Mg^{II}(H_2O)$, Zn^{II}, or Pd^{II} and M' = Pt^{II} or Pd^{II}.

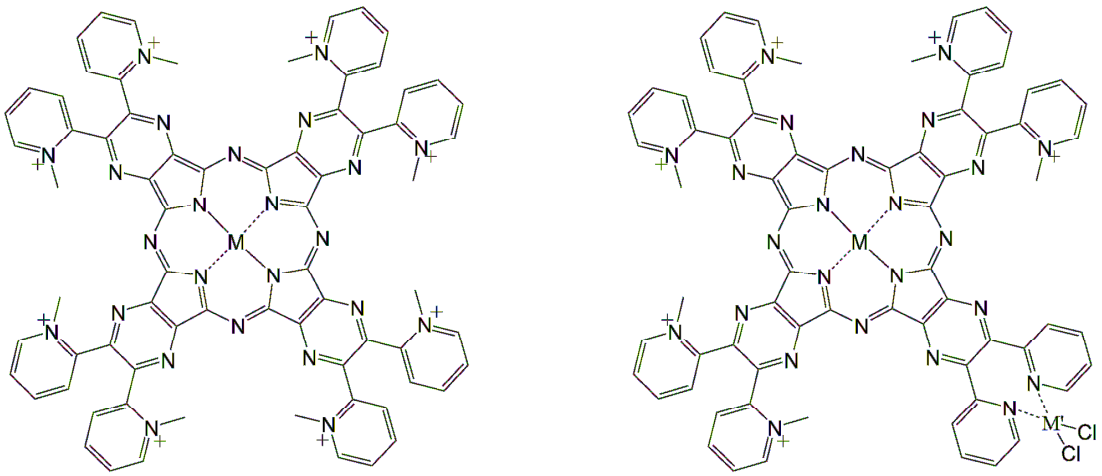

Figure 1.3. Schematic representation of the charged species A) $[(CH_3)_8LM]^{8+}$ and its corresponding hexacation B) $[(PtCl_2)(CH_3)_6LM]^{6+}$ both using I^- as a counter ion.

cannot be substituted at the meso positions of the macrocycle because the nitrogen atoms at the meso position. However, substitution can occur at one or more positions of the fused rings on phthalocyanine and the β-pyrrole position of unsubstituted porphyrazine. In contrast to the naturally occurring porphyrins, porphyrazines can only be obtained synthetically.

1.1.1 Background Electrochemistry.

Most metalloporphyrins in nonaqueous media exhibit two ring-centered reductions and two-ring centered oxidations at the conjugated π-ring system in addition to possible metal-centered reactions for redox active metal ions. On the other hand, metallophthalocyanines and metalloporphyrazines undergo two ring-centered oxidations and up to four reductions at the conjugated macrocycle under the same solution conditions with the same metal center as an analogous metalloporphyrin.[4, 5] The potential difference between the first ring-centered oxidation and the first ring-centered reduction on metallomacrocycles is defined as the electrochemical HOMO-LUMO gap. In the case of porphyrins, the HOMO-LUMO gap averages 2.25 ± 0.15 V while for MPc it is 1.75 V.[6, 7]

The HOMO-LUMO gap of metalloporphyrins varies with the type of metal ion, the macrocycle substituents, and the macrocycle planarity.[8] In the absence of a metal-centered reductions or oxidations, all of the redox processes take place at the macrocycle forming a π anion radical and dianion for the first two reductions and a π-cation radical and dication for the two oxidations. In the case of porphyrins the $E_{1/2}$ for the first and second ring-centered reductions or first and second ring-centered oxidation are separated by 0.42 ± 0.05V and 0.29 ± 0.05V, respectively.[8] It has been suggested that these potential differences along with the electrochemically measured HOMO-LUMO gap can be used as diagnostic criteria to distinguish between metal-centered and ring-centered redox processes of metalloporphyrins.

The electronegative aza bridges in phthalocyanines and porphyrazines are responsible for the anodic shift in the ring-centered reductions and oxidations reactions[2, 3] as compared to the porphyrin[9] analogues with the same metal ion. The HOMO-LUMO gap for porphyrazine was shown to be 2.14 V in non-coordinating solvents and the two reductions average a potential difference of 0.46 V.[10, 11]

1.1.2 Background UV-Visible Spectra.

Metalloporphyrins have an absorption spectrum with bands in two distinct regions. The first region is located at 300-400 nm and is typically called the B band or the Soret band. The second region is from 600-800 nm and bands in this region are typically called Q bands.[12] The absorption wavelengths will systematically change with change in the peripheral substituents of the macrocycle. UV-vis spectra of porphyrazines and its derivatives also share these characteristics but unlike porphyrins the Soret band is shifted to shorter wavelengths while the Q band is shifted to a longer wavelength with an increased molar absorptivity.[10, 11] Being a derivative of porphyrazines, metallophthalocyanines show a similar trend in absorption spectra compared to porphyrins with B bands typically in the region of 250-400 nm and Q bands near 670 nm.[13]

Porphyrazine spectroscopic and electrochemical properties make them useful as industrial pigments,[14, 15] chemical sensors,[16] fluorophors,[17] electrocatalysts,[18, 19] and as photosensitizers in photodynamic therapy (PDT).[20-29] Therefore it is very important to understand the character of the low-lying excited states, which can examine using electrochemistry and spectroelectrochemistry.

1.2 Homo/Heterobinuclear Neutral and Hexacationic Macrocycles.

Tetra-2,3-(5,6-di-2pyridylpyrazino)porphyrazines with Externally Appended Pyridine Rings

Hetero-pentanuclear Tetra-2,3-(5,6-di-2pyridylpyrazino)porphyrazines have been studied previously.[30] To better understand the contribution of the attached metal chlorides to the porphyrazine periphery the heterobinuclear analogues will be examined. The electrochemical and spectroelectrochemical properties of these macrocycles are reported in Chapter 3. These compounds are represented as [(M'Cl_2)LM] (Figure 1.2) and were investigated along with the hexacation species [(M'Cl_2)L'M]$^{6+}$ (Figure 1.3B), which is neutralized by I^- anions.

1.3 2,3-Di(2-pyridyl)-6,7-dicyano-1,4-quinoxaline, [$(CN)_2Py_2$Quin], Its Complexes [$(CN)_2Py_2$QuinMCl_2] (M = Pd^{II}, Pt^{II}) and Related Compounds

2,3-Di(2-pyridyl)-6,7-dicyano-1,4-quinoxaline, [$(CN)_2Py_2$Quin] autocylotetramerizes to give the macrocycle tetrakis-2,3-(5,6-di-2pyridylquinoxalino)porphyrazines, [Py_8TQPzH_2].[31] The structures of [$(CN)_2Py_2$Quin] and its related derivatives can be seen in Figure 1.4. The electrochemical and spectrochemical properties of [$(CN)_2Py_2$Quin] and its metallated derivatives, [$(CN)_2Py_2$Quin$PtCl_2$] and [$(CN)_2Py_2$Quin$PdCl_2$], are reported in Chapter 4 of this thesis.

1.4 Outline of Research in this Thesis

The focus of this thesis is on the electrochemistry and spectroelectrochemistry properties of porphyrazines with substituted heterocyclic rings and its corresponding precursors. Chapter 3 examines the spectroelectrochemical properties of homo/heterobinuclear neutral and hexacationic macrocycles of tetra-2,3-(5,6-di-2pyridylpyrazino)porphyrazines (compounds **3** and **4** in Figure 1.2) which are abbreviated as [(M'Cl_2)LM] and [(M'Cl_2)L'M], respectively. Chapter 4 focuses on 2,3-

di(2-pyridyl)-6,7-dicyano-1,4-quinoxaline [$(CN)_2Py_2Quin$] which is a precursor of tetrakis-2,3-(5,6-di-2pyridylquinoxalino)porphyrazines.[31]

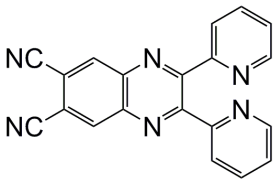

$[(CN)_2Py_2Quin]$

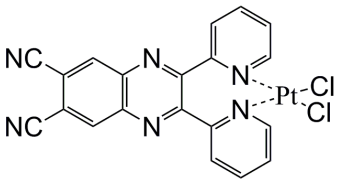

$[(CN)_2Py_2QuinPtCl_2]$

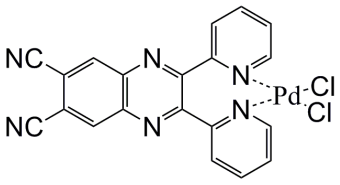

$[(CN)_2Py_2QuinPdCl_2]$

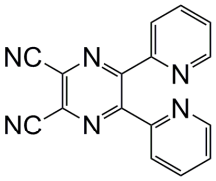

$[(CN)_2Py_2Pyz]$

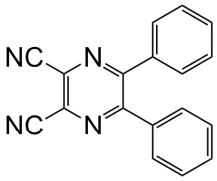

$[(CN)_2Ph_2Pyz]$

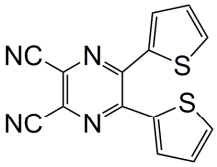

$[(CN)_2Th_2Pyz]$

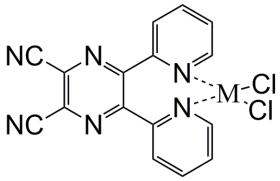

$[(CN)_2Py_2PyzMCl_2]$ ($M = Pt^{II}, Pd^{II}$)

Figure 1.4. Structures of investigated precursor molecules.

1. 5 References

1. Kadish, K. M.; Smith, K. M.; Guilard, R., Eds., *The Porphyrin Handbook*. Academic Press: San Diego, 2000; Vol. 1-10.
2. Liao, M. S.; Scheiner, S., *J. Comput. Chem.* **2002,** *23*, 1391-1403.
3. Tangen, E.; Ghosh, A., *J. Am. Chem. Soc.* **2002,** *124*, 8117-8121.
4. L'Her, M.; Pondaven, A., The Porphyrin Handbook. In Kadish, K. M.; Smith, K. M.; Guiland, R., Eds. Academic Press: San Diego, 2003; Vol. 16, pp 117-169.
5. Kobayashi, N., The Porphyrin Handbook. In Kadish, K. M.; Smith, K. M.; Guilard, R., Eds. Academic Press: San Diego, 2000; Vol. 2, pp 301-360.
6. Lever, A. B. P., Phthalocyanines: Properties and Applications. In Leznoff, C. C.; Lever, A. B. P., Eds. VCH Publishers: New York, 1993; Vol. 3, pp 1-69.
7. Kadish, K. M.; Smith, K. M.; Guilard, R., *The Porphyrin Handbook*. Academic Press: San Diego, 2000; Vol. 9.
8. Kadish, K. M.; Royal, G.; Van Caemelbecke, E.; Gueletti, L., In *The Porphyrin Handbook*, Kadish, K. M., Smith, K. M.; Guilard, R. Eds.;, Ed. Academic Press: San Diego, 2000; Vol. 9, pp 1-219.
9. Jackson, A. H., In *The Porphyrins*, Dolphin, D., Ed., Ed. Academic Press: New York, 1978; Vol. 1, pp 1-219.
10. Kobayashi, N., In *The Porphyrin Handbook*, Kadish, K. M., Smith, K. M.; Guilard, R. Eds.;, Ed. Academic Press: San Diego, 2000; Vol. 2, pp 301-360.
11. L'Her, M.; Pondaven, A., In *The Porphyrin Handbook*, Kadish, K. M.; Smith, K. M.; Guilard, R., Eds. Academic Press: San Diego, 2003; Vol. 16, pp 117-169.
12. Donzello, M. P.; Ercolani, C.; Stuzhin, P. A., *Coord. Chem. Rev.* **2006,** *250*.

13. Kadish, K. M., Smith, K. M.; Guilard, R. Eds.;, *The Porphyrin Handbook*. Academic Press: San Diego, 2003; Vol. 16.

14. Erk, P.; Hengelsberg, H., In *The Porphyrin Handbook*, Kadish, K. M., Smith, K. M.; Guilard, R., Ed. Academic Press: San Diego, 2000; Vol. 19, pp 105-149.

15. Osugi, M. E.; Carneiro, P. A.; Zanoni, M. V. B., *J. Braz. Chem. Soc.* **2003,** *14*, 660-665.

16. Kandaz, M.; Yarasir, M. N.; Guney, T.; Koca, A., *Journal of Porphyrins and Phthalocyanines* **2009,** *13*, 712-721.

17. Hammer, R. P.; Owens, C. V.; Hwang, S.-H.; Sayes, C. M.; Soper, S. A., *Bioconjugate Chem.* **2002,** *13*, 1244-1252.

18. Osmanbas, O. A.; Koca, A.; Ozcesmeci, I.; Okur, A. I.; Gul, A., *Electrochim. Acta* **2008,** *53*, 4969-4980.

19. Woehrle, D.; Suvorova, O.; Gerdes, R.; Bartels, O.; Lapok, L.; Baziakina, N.; Makarov, S.; Slodek, A., *Journal of Porphyrins and Phthalocyanines* **2004,** *8*, 1020-1041.

20. Li, H.; Jensen, T. J.; Fronczek, F. R.; Vicente, M. G. H., *J. Med. Chem.* **2008,** *51*, 502-511.

21. Fernandez, D. A.; Awruch, J.; Dicelio, L. E., *Photochem. Photobiol.* **1996,** *63*, 784.

22. Lawrence, D. S.; Whitten, D. G., *Photochem. Photobiol.* **1996,** *64*, 923.

23. Maree, S. E.; Nyokong, T., *J. Porphyrins Phthalocyanines* **2001,** *5*, 782.

24. Müller, S.; Mantareva, V.; Stoichkova, N.; Kliesch, H.; Sobbi, A.; Wöhrle., D.; Shopova, M., *J. Photoch. Photobio. B* **1996,** *35*, 167.

25. O'Conner, A. E.; Gallagher, W. M.; Byrne, A. T., *Photochem. Photobiol.* **2009,** *85*, 1053.

26. Schnurpfeil, F.; Sobbi, A. K.; Spiller, W.; Kliesch, H.; Wohrle, D., *J. Porphyrins Phthalocyanines* **1997,** *1*, 159.

27. Shinohara, H.; Tsaryova, O.; Schnurpfeil, G.; Wohrle, D. J., *Photochem. Photobiol. A* **2006,** *184*, 50.

28. Spiller, W.; Kliesch, H.; Wohrle, D.; Hackbarth, S.; Roder, B.; Schnurpfeil, G., *J. Porphyrins Phthalocyanines* **1998,** *2*, 145.

29. Szacilowski, K.; Macyk, W.; Drzewiecha-Matuszek, A.; Brindell, M.; Stochel, G., *Chem. Rev.* **2005,** *105*, 2647-2694.

30. Donzello, M. P.; Viola, E.; Ercolani, C.; Fu, Z.; Futur, D.; Kadish, K., *Inorg. Chem.* **2012,** *51*, 12548.

31. Novakova, V.; Zimcik, P.; Miletin, M.; Kopecky, K.; Musil, Z., *Eur. J. Org. Chem.* **2010**, 732-739.

CHAPTER TWO

Experimental Methods

2.1 Chemicals

High-purity nitrogen gas from Matheson was used to deoxygenate solutions before each electrochemical and spectroelectrochemical experiment. Anhydrous dimethylsulfoxide (DMSO), pyridine, and acetonitrile (AN) were obtained from Sigma Aldrich and used as received. Tetra-n-butylammonium perchlorate (TBAP) was received from Fluka Chemical Co. and dried under vacuum at 40°C for at least one week prior to use.

Porphyrazines and their corresponding quinoxaline and pyrazine precursors investived in this work were synthesized and graciously provided by Professor Claudio Ercolani's research group at the Università degli Studi di Roma "La Sapienza" in Italy.

2.2 Experimental Methods

2.2.1 Cyclic Voltammetry

Cyclic voltammetry (CV) was performed at 298 K with an EG&G model 173 potentiostat coupled with an EG&E model 175 universal programmer. Current-voltage curves were recorded on an Allen Datagraph 1000 or 1100 Series X-Y recorder. A three-electrode system was used, consisting of a glassy carbon working electrode, a platinum counter electrode, and a saturated calomel reference electrode (SCE). The reference electrode was separated from the bulk solution by a fritted-glass bridge filled with the solvent/supporting electrolyte mixture.

Measurements by Cyclic Voltammetry. First, a background CV is taken to determine the useable potential window of the solvent containing 0.1 M TBAP and to ensure that the system is electrochemically "clean" in that window. After taking the background voltammogram, ferrocene (Fc) is added to the electrolyte solution, for use as

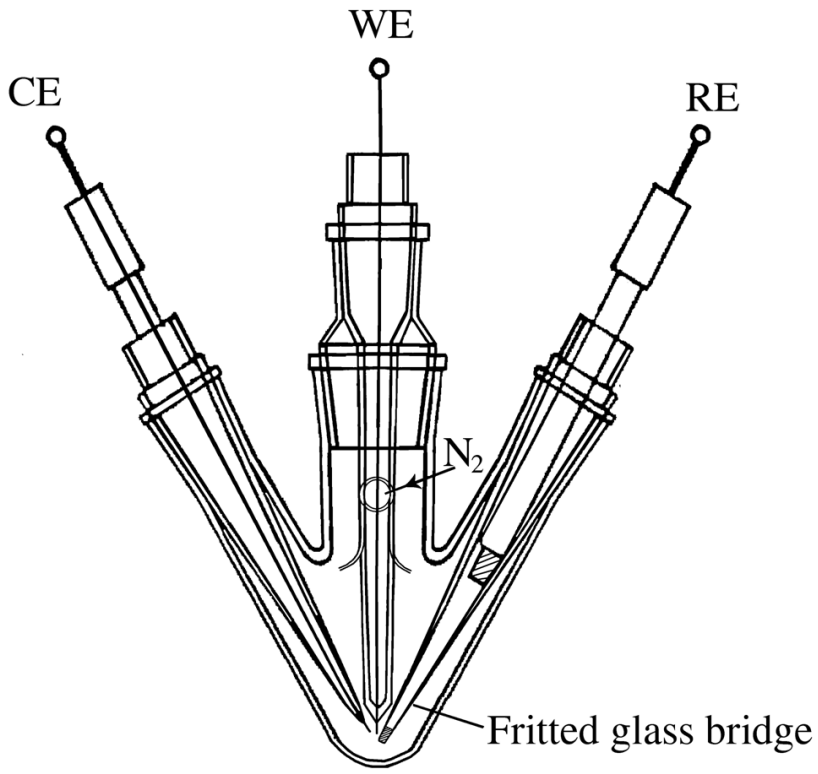

Figure 2.1. Schematic illustration of the home-made electrochemical cell utilized and the three-electrode system used for each electrochemical experiment: WE, CE and RE are the working, counter and reference electrodes, respectively. The reference electrode was put into the fritted glass bridge and Teflon tubing was inserted in the N_2 entrance for deoxygenation.[1]

an internal standard, and its oxidation is used to determine the condition of the reference electrode. Once the condition of the reference electrode has been verified, the cell, working electrode, counter electrode and the fritted glass bridge are rinsed with acetone and dried. A 1 mL solution of the analyte in the TBAP solution, with a concentration ranging from 0.5 – 0.1 mM, is added to the cell and its CV is taken.

2.2.2 Spectroelectrochemistry

UV-visible spectroelectrochemistry is a hybrid technique that utilizes UV-visible spectroscopy to monitor the products of electrochemical reactions in-situ. A home-made thin-layer cell equipped with a light transparent platinum gauze working electrode (Figure 2.2) was used to perform UV-vis spectroelectrochemical experiments.[2] Potentials were applied and monitored using an EG&G Model 173 Potentiostat. A Hewlett-Packard Model 8453 diode array rapid-scanning spectrophotometer was used to acquire time-resolved UV-visible spectra.

The utilized HP 8453 spectrophotometer is a single-beam instrument with collimating optics. A deuterium-discharge and tungsten lamp combination are used to generate light in the ultraviolet (UV) and the visible and short wave near infrared range, respectively. The emitted light of the deuterium lamp ranges from 190 nm to approximately 800 nm while the tungsten lamp has a range of 370 nm to 1100 nm wavelength range for the tungsten lamp. The diode array consists of a series of 1024 individual photodiodes and control circuits etched onto a semiconductor chip, with a wavelength range from 190 to 1100 nm and a nominal sampling interval of 0.9 nm.

Absorbance is defined by Beer's law as $A = \varepsilon bc$, where A, is the absorbance, b is the cell pathlength and c is concentration of the sample in moles per liter (M). The molar

absorptivity, ε, has units of $M^{-1}cm^{-1}$.

Measurement of UV-Visible Spectra. The initial steps of a spectroelectrochemical experiment are similar to what is described above for cyclic voltammetry. The spectroelectrochemical cell, shown in Figure 2.2, is filled with 4.0 mL of a 0.2 M TBAP solution and purged with nitrogen gas for 2 minutes. The electrochemical background is then taken followed by the UV-vis spectra of the blank. The analyte is then dissolved in 1 mL of 0.2 M TBAP solution and added to the spectroelectrochemical cell, with nitrogen being bubble through the solution for 30 seconds. After the solution has been mixed and degassed (via bubbling nitrogen gas), the initial neutral spectra is taken.

A thin-layer cyclic voltammogram (TLCV) is then taken to determine the potential at which each redox process occurs. After determining where each redox process occurs, the potentiostat is programmed to hold the potential at a voltage where the analyte is not reduced or oxidized. Another spectra is taken to make sure there are not other chemical processes occurring before the redox process which cannot be observed electrochemically. Simultaneously, the potential is switched to a potential beyond $E_{1/2}$ and spectra are continuously taken until the spectral changes become negligible. The potential is then set back to the initial potential to check the reversibility of the process, i.e. to verify the presence or absence of coupled chemical reactions associated with electron transfer. These steps are performed for each subsequent redox process by stepping the potential before and after each process and then stepping the potential back in the reverse order.

2.2.3 Theoretical Calculations

All quantum chemical calculations of the investigated compounds were provided by Dr. Enrico Bodo from the Dipartimento di Chimica, Università degli Studi di Roma in Italy. DFT and TDDFT calculations were performed to provide both gas phase structures and absorption spectra of all compounds considered in this thesis. The calculations were done with Gaussian09. Geometry optimizations have been carried out using the B3LYP functional[3] and the 6-311+G(d)[4] basis set for the first and second row atoms and the LANL ECP with a TZ basis on the metal atoms.[5] Three different approaches were used for calculation of the electronic spectra: a) for the neutral unmetalated compounds, the excited state calculations were performed by means of the TDDFT method[6] using the above basis sets and the B3LYP functional; b) for the metalated compounds the M06X2 was used,[7] since the B3LYP gave a poor performance with respect to experimental data and; c) for the anionic molecules, the BMK functional[8] provided quite a satisfactory agreement with the experimental spectra. The calculations of the anionic molecules were performed using the unrestricted Kohn and Sham method for a doublet multiplicity molecule.

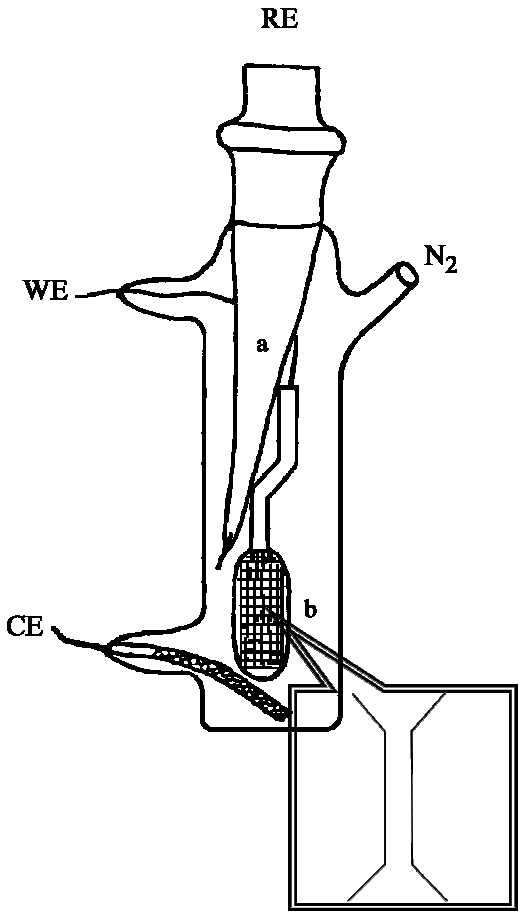

Figure 2.2 Schematic illustration of thin-layer UV-visible spectroelectrochemical cell.

2.3 References

1. Chen, P. Electrochemical and Spectroelectrochemical Studies of Porphyrin, Corrole and Porphycenes. Ph.D. Dissertation, University of Houston, Houston, TX, 2009.
2. Lin, X.; Kadish, K. M., *Anal. Chem.* **1985,** *57*, 1849.
3. Becke, A. D., *J. Chem. Phys.* **1993,** *98*, 5648.
4. McLean, A. D.; Chandler, G. S., *J. Chem. Phys.* **1980,** *72*, 5639.
5. Hay, P. J.; Wadt, W. R., *J. Chem. Phys.* **1985,** *82*, 299.
6. Casida, M. E.; Jamorski, C.; Casida, K. C.; Salahub, D. R., *J. Chem. Phys.* **1998,** *108*, 4439.
7. Zhao, Y.; Truhlar, D. G., *Theor. Chem. Acc.* **2008,** *120*, 215.
8. Boese, A. D.; Martin, J. M. L., *J. Chem. Phys.* **2004,** *121*, 3405.

CHAPTER THREE

Tetra-2,3-pyrazinoporphyrazines with Externally Appended Pyridine Rings. UV-Visible and Electrochemical Behavior of Homo/Heterobinuclear Neutral and Hexacationic Macrocycles

3.1 Introduction.

As part of our previous studies on porphyrazine macrocycles, we have focused on a series of compounds which were shown to be excellent photosensitizers [1, 2] for the generation of singlet oxygen, $^1O_2$, the cytotoxic agent active in photodynamic therapy (PDT), a well known anticancer therapy.[3-7] The investigated porphyrazines in their monometallic form are represented as [LM] where L = tetrakis-2,3-[5,6-di(2-pyridyl)pyrazino]porphyrazinato anion and M = Zn^{II}, $Mg^{II}(H_2O)$ and Pd^{II}. In addition to the monometallic compounds, a series of uncharged homo/hetero binuclear and pentanuclear species also behave as highly photoactive materials for $^1O_2$ production. These compounds are represented as $[(M'Cl_2)LM]$,[2] and $[(M'Cl_2)_4LM]$[1, 8, 9] where M' = Pd^{II} or Pt^{II} and M = Zn^{II}, $Mg^{II}(H_2O)$ or Pd^{II}. In addition to the binuclear complexes $[(M'Cl_2)LM]$, related monoplatinated hexacations formulated as $[(PtCl_2)(CH_3)_6LM]^{6+}$ (charge-balanced with I^- ions), endowed with moderate-to-low water solubility ($\leq 5\cdot10^{-5}$ M) were also prepared and studied.[2] Due to the good response of the hexacations in terms of $^1O_2$ quantum yields, the Zn^{II} charged species $[(PtCl_2)(CH_3)_6LZn]^{6+}$ (Chart 3.1A) and its related octacation $[(CH_3)_8LZn]^{8+}$ (Chart 1B), both neutralized by I^- ions, were examined as to their interaction with a telomeric DNA G-quadruplex (G4) structure in a K^+ rich water solution.[10, 11] This resulted in both cases in the formation of a 2:1 Zn^{II}-complex/G4 structural arrangement in which the G-quadruplex was highly stabilized in its "parallel" conformation.

Both charged species in Chart 3.1 were shown to interact in water with a 21-mer double strand sequence taken as a model for B-DNA under the specified experimental

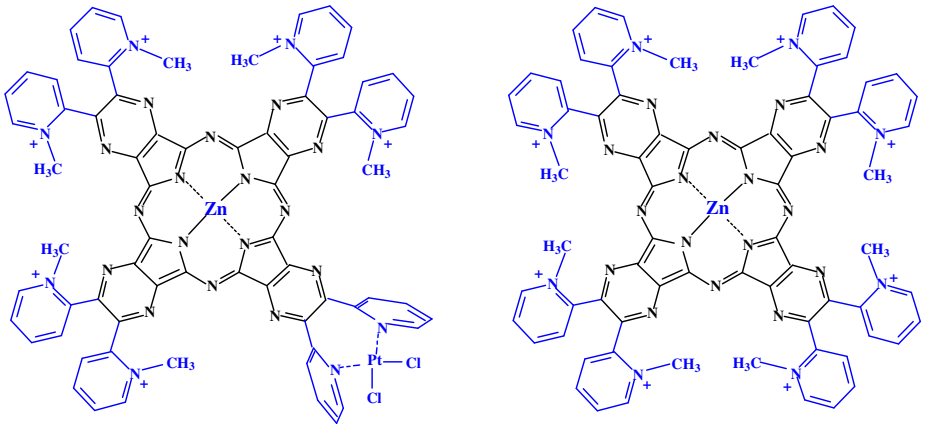

Chart 3.1. Schematic representation of the Zn^{II} charged species A) $[(PtCl_2)(CH_3)_6LZn]^{6+}$ and B) its corresponding octacation $[(CH_3)_8LZn]^{8+}$ (using I^- as counter-ions).

conditions.[12] Noteworthy, the $[(PtCl_2)(CH_3)_6LZn]^{6+}$ hexacation incorporates peripherally a cis-platin-like functionality, thus opening up new possibilities for applications in the area of chemotherapy and qualifying the complex as a potential multimodal anticancer agent. Based on this information, it was of interest to examine the redox behavior of the Zn^{II} cation $[(PtCl_2)(CH_3)_6LZn]^{6+}$ and its $Mg^{II}(H_2O)$ and Pd^{II} analogs and to then compare these data to that of the related neutral complexes $[(M'Cl_2)LM]$ in a nonaqueous solvent (DMSO). We also wished to compare the electrochemical and spectroscopic data for these compounds to what was earlier reported for the series of mononuclear [LM][13-15] and pentanuclear derivatives of the type $[(M'Cl_2)_4LM]$,[8, 9, 15, 16] and salt-like species, $[(CH_3)_8LM](I)_8$,[13, 15] where M = $Mg^{II}(H_2O)$, Zn^{II} or Pd^{II} and M' = Pd^{II} or Pt^{II}. Structures of [LM], $[(M'Cl_2)LM]$ and $[(M'Cl_2)_4LM]$ compounds are shown in Chart 3.2. Redox properties of the porphyrazines in Charts 3.1B, 3.2A and 3.2C were earlier examined by cyclic voltammetry and thin-layer UV-visible spectroelectrochemistry in DMSO containing 0.1 M tetrabutylammonium perchlorate (TBAP)[8, 13, 15, 16] and, in the present study, the dimetallic compounds in Charts 3.1A and 3.2B are now examined under the same solution conditions. The results for all five series of porphyrazines in Charts 3.1 and 3.2 are then compared to elucidate the most important factors determining the ease of reduction and spectroscopic properties of a given compound. this table also includes data previously reported for [LM], $[(PtCl_2)_4LM]$, $[(PdCl_2)_4LM]$ and $[(CH_3)_8LM]^{8+}$under the same solution conditions.[8, 13, 15, 16]

3.2 Results and Discussion

3.2.1 UV-visible spectral behavior

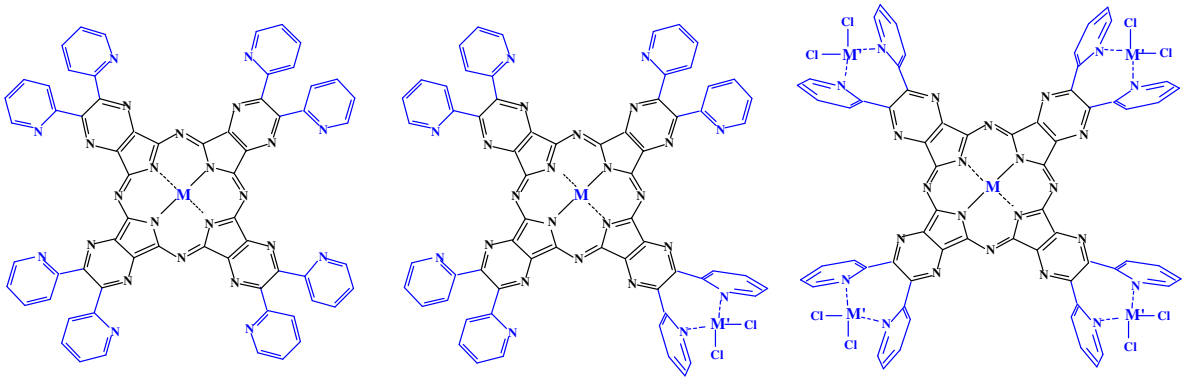

Chart 3.2. Schematic representations of (A) [LM], (B) [(M'Cl_2)LM], and (C) [(M'Cl_2)$_4$LM], where M = $Mg^{II}(H_2O)$, Zn^{II}, or Pd^{II} and M' = Pt^{II} or Pd^{II}.

Previous studies on the interaction of the bimetallic $[(PtCl_2)(CH_3)_6LZn]^{6+}$ species with both the 21-mer telomeric G-quadruplex structure and with a double strand (ds) B-DNA model, indicate that the hexacation exists in an equilibrium between a monomer and a dimer in a buffered water solution, under mimicked physiological conditions (excess of K+ ions, pH 7.4). The UV-visible spectrum of this monomer/dimer mixture is characterized by intense peaks of comparable intensity in the Q-band region at 625 and 650 nm. Assignment of the lower energy peak (650 nm) to the monomer is supported by density functional theory (DFT) and time-dependent DFT (TDDFT) calculations.[12] The UV-visible spectra of the same bimetallic hexacation in pure water (Figure 3.1A) show that dilution of the solution in the range of 10^{-5}-10^{-7} M only partly shifts the equilibrium in the direction of the monomer. Noteworthy, this bimetallic complex is totally monomeric in DMSO[12] and exhibits a narrow Q band at 666 nm in the absence of supporting electrolyte (Figure 3.1A). The same band appears at 663 nm in DMSO containing 0.1 M TBAP (Figure 3.2A) with this difference being attributed to the difference in ionic strength between the two solutions. As can be seen in Figures 3.1, 3.2 and Table 3.1, similar spectral features are observed for the Mg^{II} and Pd^{II} hexacations in DMSO. Of more importance, however, is the fact that the compounds are partly aggregated in aqueous solutions and mainly monomeric in DMSO or DMSO containing 0.1 M TBAP. Our findings also indicate that aggregation of the hexacations in water is dependent of the type of central metal ion, being smallest in the case of the Zn^{II} porphyrazine and largest for the Pd^{II} derivative.

UV-visible spectral data for the triad of charged bimetallic species

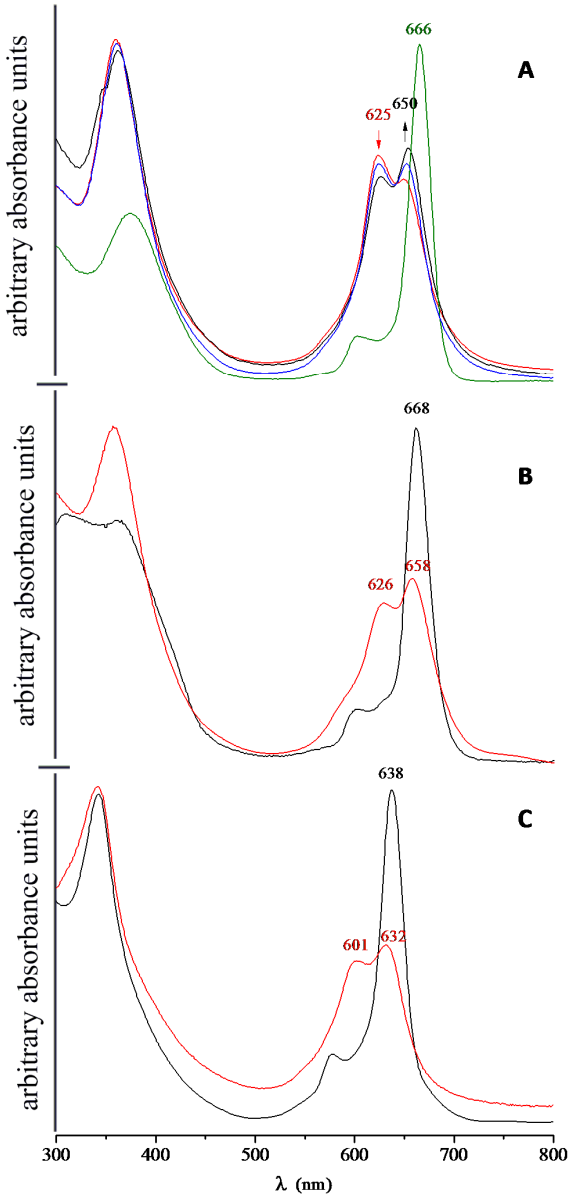

Figure 3.1. UV-visible spectra of: A) $[(PtCl_2)(CH_3)_6LZn]^{6+}$ in DMSO (green line) and in H_2O at different concentrations: $5x10^{-5}$ M (red line); $5x10^{-6}$ M (blue line); $5x10^{-7}$ M (black line); B) $[(PtCl_2)(CH_3)_6LMg(H_2O)]^{6+}$ in DMSO (black line) and in H_2O (c = $4.1x10^{-5}$ M; red line) and C) $[(PtCl_2)(CH_3)_6LPd]^{6+}$ in DMSO (black line) and in H_2O (c = $5.8x10^{-5}$ M; red line).

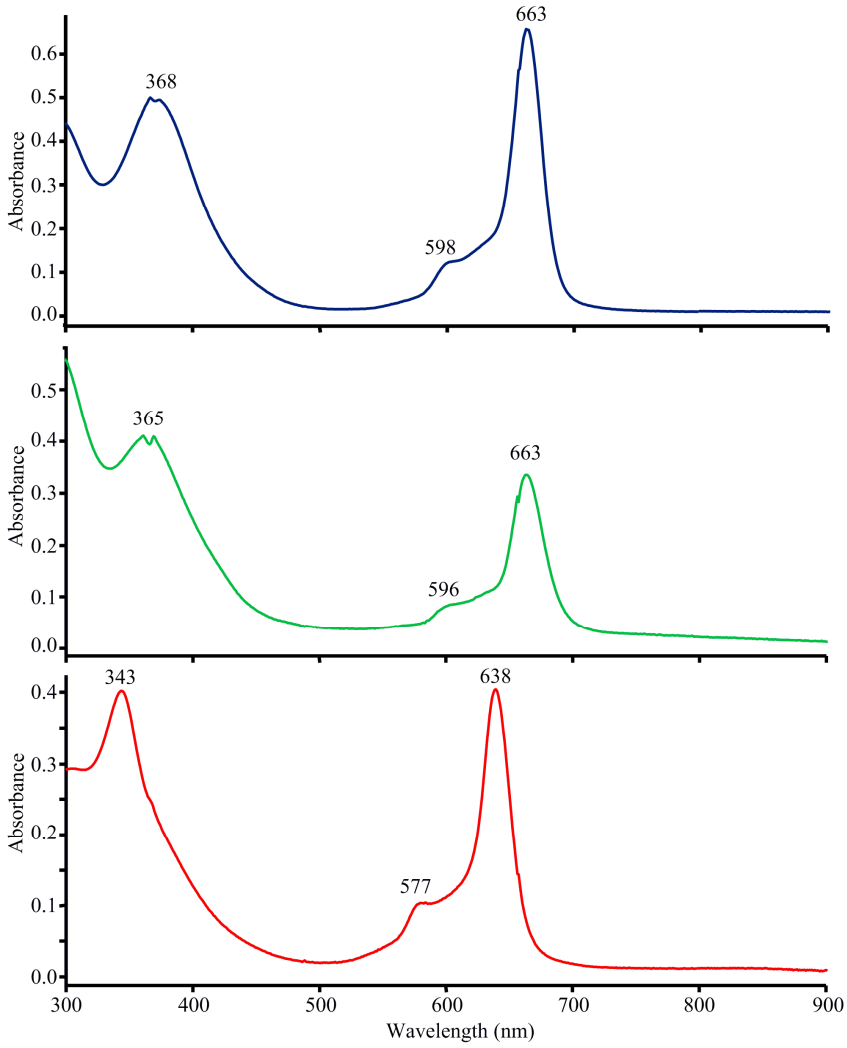

Figure 3.2. UV-visible spectra of $[(PtCl_2)(CH_3)_6LZn]^{6+}$(top), $[(PtCl_2)(CH_3)_6LMg(H_2O)]^{6+}$ (middle) and $[(PtCl_2)(CH_3)_6LPd]^{6+}$ (bottom) in DMSO, containing 0.1 M TBAP.

$[(PtCl_2)(CH_3)_6LM]^{6+}$ (M = Zn^{II}, $Mg^{II}(H_2O)$, Pd^{II}) in DMSO and water solutions are listeds in Table 3.1 together with spectral data for the neutral analogs $[(M'Cl_2)LM]$ (M' = Pd^{II}, Pt^{II}) and the related mononuclear, pentanuclear and octacationic complexes. A look at the Q-band positions for the compounds in Tables 3.1 allows for some interesting observations. First, within the series of the three species having the formula [LM], $[(PdCl_2)LM]$ and $[(PtCl_2)LM]$ only a small Q-band peak variation is observed ($\leq$ 5 nm).

This indicates that external mono-metalation of $PtCl_2$ or $PdCl_2$ has little or no effect on the Q-band position. In contrast to the minimal effect of the $PdCl_2$ or $PtCl_2$ group on the UV-visible spectra, a quite significant variation in the spectra is seen upon changing the central metal ion from Mg^{II} or Zn^{II} to Pd^{II}. For example, the most intense Q band of [LM] is located at 653-655 nm for the Mg^{II} and Zn^{II} derivatives and at 633 nm for the Pd^{II} complex. The same trend in λ_{max} is seen for metalloporphyrazines in the related series of compounds of Table 3.1 and this is most evident in the case of the triad of cations $[(PtCl_2)(CH_3)_6LM]^{6+}$ (M = $Mg^{II}(H_2O)$, Zn^{II}, Pd^{II}) for which the Q-band maximum is located at 666-668 nm for the Mg^{II} and Zn^{II} species and at 638 nm for the Pd^{II} complex in DMSO. The B (Soret) band is also shifted by 21-31 nm for the Pd^{II} hexacation compared to the Mg^{II} and Zn^{II} complexes. This trend is consistent with similar reported shifts in the absorption bands of the couples of Pd^{II} and Zn^{II} porphyrin complexes [(TPP)Pd] and [(TPP)Zn],[17] [(OEP)Pd] and [(OEP)Zn],[18] or $[(F_{20}TPP)Pd]$ and $[F_{20}OEPZn]$.[19] For these three series of Pd^{II} and Zn^{II} compounds the shift in wavelengths amounts to 20-25 nm for the couples of Zn^{II} and Pd^{II} compounds and can be explained by the much stronger metal perturbation on the (π,π*) transitions of the Pd^{II} derivative as

Table 3.1. UV-Visible spectra of the complexes in DMSO and water.

Compound	Solvent	λ_{max} [nm] (logε) Soret region		Q-band region				Ref[a]
[LZn]	DMSO	372 (5.10)		565sh (4.02)	592 (4.54)	629sh (4.61)	655 (5.36)	13
[($PdCl_2$)LZn]	DMSO	371 (5.01)			592 (4.43)		655 (5.20)	2
[($PtCl_2$)LZn]	DMSO	377 (4.91)			597 (4.32)		660 (5.22)	2
[($PtCl_2$)(CH_3)$_6$LZn]$^{6+}$	DMSO	372 (4.85)			602 (4.32)		666 (5.16)	2
	H_2O	360 (4.82)				625 (4.64)	650 (4.59)	tw
[($PdCl_2$)$_4$LZn]	DMSO	370 (5.03)			598 (4.47)		657 (5.23)	8
[($PtCl_2$)$_4$LZn]	DMSO	382 (4.91)			603 (4.44)		667 (5.3)	8
[(CH_3)$_8$LZn]$^{8+}$	DMSO	373 (4.37)			600sh(3.86)	637sh (3.89)	666 (4.74)	13
[LMg(H_2O)]	DMSO	374 (5.08)		565sh (3.96)	594 (4.36)	629sh (4.55)	653 (5.34)	13
[($PdCl_2$)LMg(H_2O)]	DMSO	373 (5.02)			595 (4.45)		653 (5.62)	2
[($PtCl_2$)LMg(H_2O)]	DMSO	370 (4.89)			592 (4.29)	621sh (4.27)	653 (5.07)	2
[($PtCl_2$)(CH_3)$_6$LMg(H_2O)]$^{6+}$	DMSO	362 (4.58)			602 (4.00)		668 (4.08)	2
	H_2O	357 (4.79)				626 (4.47)	658 (4.53)	tw
[($PdCl_2$)$_4$LMg(H_2O)][a]	DMSO	342	368sh		597		656	8
[($PtCl_2$)$_4$LMg(H_2O)]	DMSO	385 (4.71)			600 (4.22)	628sh (4.26)	659 (5.00)	8
[(CH_3)$_8$LMg(H_2O)]$^{8+}$	DMSO	370 (4.83)	415sh (4.56)	565sh (3.80)	600 (4.33)	630sh (4.33)	660 (5.15)	13
[LPd]	DMSO	340 (4.94)	380sh (4.58)		575 (4.32)		633 (4.95)	15
[($PdCl_2$)LPd]	DMSO	341 (4.99)			575 (4.35)		636 (4.99)	2
[($PtCl_2$)LPd]	DMSO	341 (4.97)	399sh (4.48)		574 (4.38)		635 (4.98)	2
[($PtCl_2$)(CH_3)$_6$LPd]$^{6+}$	DMSO	341 (4.85)			578 (4.23)		638 (4.86)	2
	H_2O	342 (3.64)			601 (3.34)		632 (3.38)	tw
[($PdCl_2$)$_4$LPd]	DMSO	341 (5.02)	370sh 4.69)		575 (4.34)		636 (5.03)	15
[($PtCl_2$)$_4$LPd]	DMSO	345 (5.00)			580 (4.44)		639 (5.10)	8
[(CH_3)$_8$LPd]$^{8+}$	DMSO	342 (5.04)	380sh (4.63)		571 (4.41)		638 (5.14)	15

[a]tw = this work

compared to that of Zn^{II} compound.[20] Typically reducing the symmetry of porphyrazine (D_{4h}) leads to the splitting of the Q band. [21-24] The external appendage of $PtCl_2$ to the macrocycle reduces the overall symmetry of the macrocycle. This should lead to splitting of the Q band absorption but this is not observed for all the metal derivatives. A similar phenomenon was observed by Zimcik et al[25] for tetrapyrazinoporphyrazines withdifferent numbers of pyridyl rings attached to the periphery. The absence of spectral changes because of the decrease in symmetry is an indication that the attached pyridyl system only weakly interacts with macrocycle's conjugated system.

Comparisons can also be made between the UV-visible spectra of the [LM] and $[(PtCl_2)(CH_3)_6LM]^{6+}$ complexes in DMSO (Table 3.1). In this case, a significant bathochromic shift of 10-15 nm is observed in the Q band position upon formation of the hexacations $[(PtCl_2)(CH_3)_6LM]^{6+}$ from [LM] when M = $Mg^{II}(H_2O)$ or Zn^{II} but a smaller shift of 5 nm is seen when M = Pd^{II}. Thus, the Zn^{II} and Mg^{II} hexacation spectra are quite similar to each other in DMSO, but differ significantly from the spectrum of the Pd^{II} hexacation which has bands at 341, 578 and 638 nm and very closely resembles spectra of the three uncharged Pd^{II} compounds in neat DMSO. This result is in line with previous findings concerning the changes which occur upon going from the mononuclear to the pentanuclear species[8, 15, 16] or to the octacations.[13, 15]

The above described UV-visible data confirm that external quaternization increases peripheral delocalization of the negative charge of the macrocycle with a consequent increase of its electron deficiency but the exact effect will be highly influenced by the type of central metal (Mg, Zn or Pd) and its electronegativity, which

varies from 1.31 for Mg^{II} to 2.20 for Pd^{II}.[26] This important aspect is further supported by the electrochemical data discussed below. Finally, a hypsochromic shift of the Q band is observed for the hexacations upon going from DMSO to aqueous solutions, with the magnitude of the shift in λ_{max} being 16 nm in the case of M = Zn^{II}, 10 nm in the case of M = Mg^{II} and 6 nm for the Pd^{II} porphyrazine (see Table 3.1). The difference in the λ_{max} may be related to the strength of axial ligand binding, which is largest for Zn^{II} and smallest, or non-existent, for Pd^{II}.[27]

3.2.2 Electrochemistry.

Cyclic voltammetric and spectroelectrochemical measurements were carried out in DMSO on the three series of compounds [$(PdCl_2)$LM], [$(PtCl_2)$LM] and [$(PtCl_2)(CH_3)_6$LM]$^{6+}$, where M = $Mg^{II}(H_2O)$, Zn^{II} or Pd^{II}. Examples of cyclic voltammograms illustrating the first two reductions of each compound in DMSO are shown in Figure 3.3 which also includes cyclic voltammograms for the [LM] and [$(PtCl_2)_4$LM] complexes with the same central metal ions. Potentials for each redox process of the newly investigated compounds in DMSO are summarized in Table 3.2 and this table includes data previously reported for [LM], [$(PtCl_2)_4$LM], [$(PdCl_2)_4$LM], and [$(CH_3)_8$LM]$^{8+}$ under the same solution conditions.[8, 13, 15, 16]

Two types of electrochemical behavior are observed for the porphyrazines investigated in our laboratory. One is for [LM], [$(PdCl_2)$LM], and [$(PtCl_2)$LM] and the other for [$(PtCl_2)(CH_3)_6$LM]$^{6+}$, [$(PdCl_2)_4$LM], [$(PtCl_2)_4$LM] and [$(CH_3)_8$LM]$^{8+}$. The data for these six series of compounds is discussed below, both as a function of the central metal ion while keeping the macrocycle constant and as a function of the

macrocycle while keeping the central metal ion constant. This is then followed by a discussion of the spectroelectrochemistry.

It should be noted that all of the compounds examined in the current study were soluble in DMSO at the concentrations necessary for electrochemical analysis (ca. 10^{-4} M or higher) but mild aggregation existed for some of the Zn^{II} compounds and more extensive aggregation was present for the Pd^{II} neutral derivatives. As described in the literature,[28] the redox potentials of the most highly aggregated compounds were determined by first scanning in a negative direction to break up the aggregates in solution after formation of the porphyrazine dianion or trianion, after which the potential was reversed and scanned in a positive direction to measure the half wave potentials and UV-visible spectra of each electroreduced species in its monomeric form.

[LM], [($PdCl_2$)LM], and [($PtCl_2$)LM]. The electrochemistry of the $Mg^{II}(H_2O)$, Zn^{II} and Pd^{II} porphyrazines with zero and one externally coordinated $PtCl_2$ or $PdCl_2$ group is illustrated by the top nine cyclic voltammograms in Figure 3.3. The three examined [LM] derivatives with $Mg^{II}(H_2O)$, Zn^{II} and Pd^{II} central metal ions undergo four reversible macrocycle-centered reductions in DMSO, but the situation is more complicated for the [($PdCl_2$)LM] and [($PtCl_2$)LM] derivatives where the third and fourth reductions are irreversible in some cases and involve chemical reactions coupled to the electron transfer in others. For this reason our comparison of the electrochemical behavior of these compounds is limited in this paper to the first two one-electron additions, where the cyclic voltammograms leading to formation of the porphyrazine anion radicals and dianions were generally well-defined.

As seen in Figure 3.3 and Table 3.3, the first reduction of [($PtCl_2$)LMg(H_2O)] and [($PdCl_2$)LMg(H_2O)] in DMSO are located at the same potential of $E_{1/2}$ = -0.37 V, as compared to $E_{1/2}$ = -0.33 V vs SCE for the first reduction of [LMg(H_2O)] under the same solvent condition.[13] Similar half wave potentials are also seen for the second reduction of [LMg(H_2O)] (-0.70 V), [($PdCl_2$)LMg(H_2O)] (-0.72 V) and [($PtCl_2$)LMg(H_2O)] (-0.73 V), giving a relatively constant $\Delta E_{1/2}$ of 350-370 mV for the three related compounds with the same central metal ion.

It was initially anticipated that the external addition of a single $PdCl_2$ or $PtCl_2$ group to [LM] would shift the potential for reduction of the macrocycle towards an easier electron addition but this is not the case for formation of the porphyrazine anion radical or dianion for M = $Mg^{II}(H_2O)$, Zn^{II} and Pd^{II}. To further verify this, all the measured potentials were adjusted to an internal standard, ferrocene (Fc), to remove the influence of liquid junction potentials from the measurement (see Table 3.3 and Figures 3.4 and 3.5).[29]

Like in the case of the above discussed $Mg^{II}(H_2O)$ derivatives, there is a relatively constant potential separation between the first and second reductions of the uncharged porphyrazines. The measured separations between the first two reductions ranges from 350-370 mV for the three neutral complexes containing $Mg^{II}(H_2O)$ and this can be compared to $\Delta E_{1/2}$ values of 390-410 mV for the Zn^{II} complexes of [LM], [($PdCl_2$)LM] and [($PtCl_2$)LM] and a $\Delta E_{1/2}$ of 320-350 mV for the Pd^{II} derivatives of these same three macrocycles. A comparison of cyclic voltammograms for the $Mg^{II}(H_2O)$ complexes with zero, one and four externally coordinated $PtCl_2$ or $PdCl_2$ groups is shown

Table 3.2. Electrochemistry of porphyrazine derivatives in DMSO, 0.1 M TBAP.

Compound	Reductions vs SCE				ΔE_{1-2}	Ref.[a]
	First	Second	Third	Fourth		
$[LMg(H_2O)]$	-0.33	-0.70	-1.39	-1.67	0.37	13
$[(PdCl_2)LMg(H_2O)]$	-0.37	-0.72			0.35	tw
$[(PtCl_2)LMg(H_2O)]$	-0.37	-0.73			0.36	tw
$[(PtCl_2)(CH_3)_6LMg(H_2O)]^{6+}$	-0.17	-0.49	-0.83		0.32	tw
$[(PdCl_2)_4LMg(H_2O)]$	-0.15					16
$[(PtCl_2)_4LMg(H_2O)]$	-0.15	-0.49	-1.12	-1.33	0.34	8
$[(CH_3)_8LMg(H_2O)]^{8+}$	-0.19	-0.47	-0.84	-1.28	0.28	13
[LZn]	-0.26	-0.67	-1.38	-1.64	0.41	13
$[(PdCl_2)LZn]$	-0.32	-0.71	-1.43	-1.67	0.39	tw
$[(PtCl_2)LZn]$	-0.30	-0.59			0.29	tw
$[(PtCl_2)(CH_3)_6LZn]^{6+}$	-0.13	-0.49	-0.97 [a]	-1.34 [b]	0.36	tw
$[(PdCl_2)_4LZn]$	-0.13	-0.54	-1.39	-1.63	0.41	16
$[(PtCl_2)_4LZn]$	-0.10	-0.45	-1.10 [a]		0.35	8
$[(CH_3)_8LZn]^{8+}$	-0.10	-0.44	-0.81	-1.24	0.34	13
[LPd]	-0.26	-0.60	-1.26	-1.61	0.34	15
$[(PdCl_2)LPd]$	-0.25	-0.60			0.35	tw
$[(PtCl_2)LPd]$	-0.24	-0.56	-1.20[a]	-1.71 [a]	0.32	tw
$[(PtCl_2)(CH_3)_6LPd]^{6+}$	-0.16[c]	-0.36	0.64[a]			tw
$[(PdCl_2)_4LPd]$	0.00	-0.37	-1.24	-1.59	0.37	15
$[(PtCl_2)_4LPd]$	0.00	-0.35	-0.97		0.35	8
$[(CH_3)_8LPd]^{8+}$	0.08	-0.33			0.41	15

[a] tw = this work. [b] Irreversible peak; value is peak potential E_p at a scan rate of 0.1 V/s. [c] $E_{1/2}$ value taken from the TLCV since it could not seen in the regular CV.

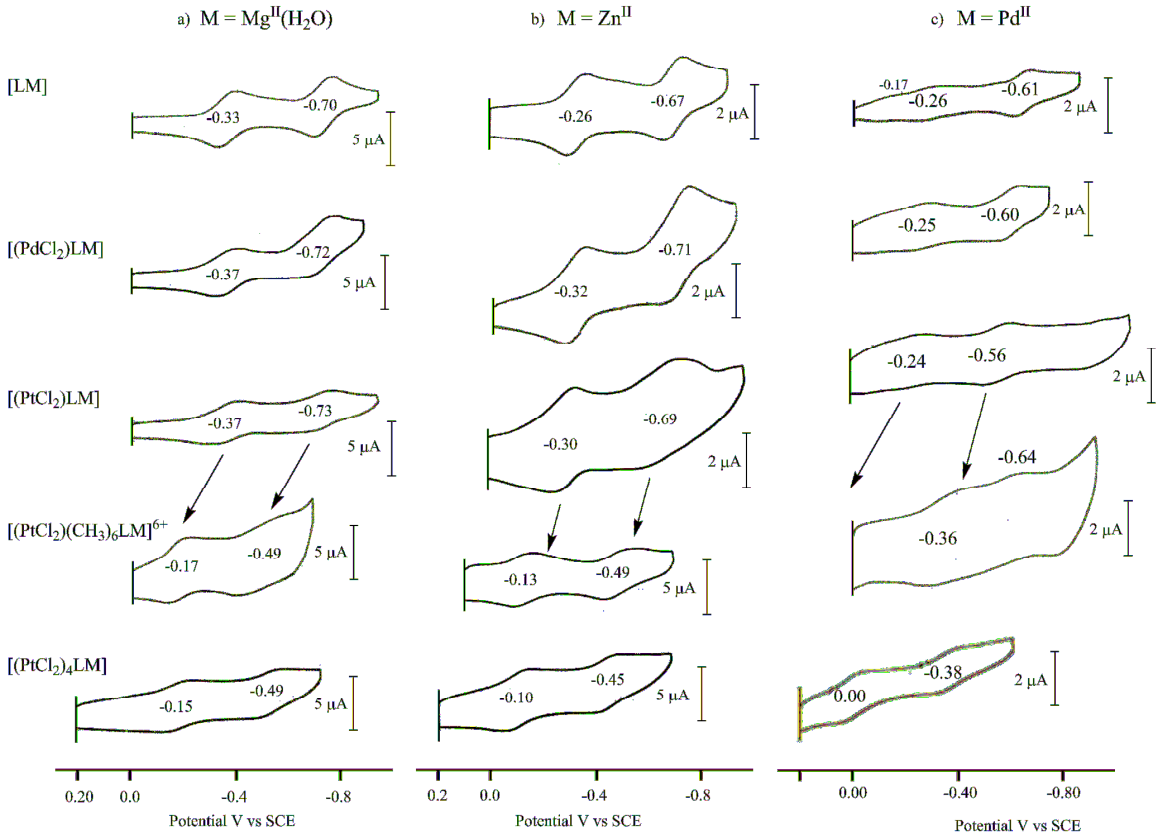

Fig. 3.3. Cyclic voltammograms illustrating the first two reductions of the species [LM], $[(PdCl_2)LM]$, $[(PtCl_2)LM]$, $[(PtCl_2)(CH_3)_6LM]^{6+}$ and $[(PtCl_2)_4LM]$ in DMSO, 0.1 M TBAP.

in Figure 3.4 where the data is plotted as $E_{1/2}$ vs the Fc/Fc^+ couple. All of the examined compounds undergo four macrocycle-centered reductions in this solvent, but only the first two are illustrated for the compounds with externally coordinated $PtCl_2$ or $PdCl_2$ groups. As seen in the figure, the first and second reductions of [$(PtCl_2)$LMg] and [$(PdCl_2)$LMg] in DMSO are located at $E_{1/2}$ = -0.81 and -1.17 V and are shifted anodically by 20 and 30 mV, respectively, compared to the reductions of [LMg] (-0.83 and -1.20 V) under the same solvent conditions. Further reductions of the bi- and penta-metallic species are not shown in Figure 3.4 because the $PdCl_2$ group on the porphyrazine is reduced after the second macrocycle-centered reduction and the last two reductions of the $PdCl_2$ derivatives actually correspond to the third and fourth reductions of [LMg].

Appending four $PtCl_2$ units to the macrocycle of [LMg] leads to [$(PtCl_2)_4$LMg] which is reduced at -0.60 and -0.94 V vs Fc/Fc^+. These reduction potentials are shifted anodically by 230 and 260 mV as compared to [LM] which is reduced at $E_{1/2}$ = -0.83 and -1.20 V vs Fc/Fc^+ (see Figure 3.4). If each of the four $PtCl_2$ units on $(PtCl_2)_4$LMg has an equal affect in shifting the reduction potentials of the porphyrazine, then a single terminal $PtCl_2$ group on the compound would theoretically result in an anodic shift of 57-65 mV for the reduction of [$(PtCl_2)$LM] as compared to the parent compound. In fact, the experimentally measured anodic shift in reduction potential upon going from [LM] to [$(PtCl_2)$LM] is only 20 mV as seen in Figure 3.4. This would indicate that multiple $PtCl_2$ units are needed to perturb the electron distribution of the macrocycle.

Cyclic voltammograms of the neutral Zn(II) complexes are illustrated in Figure 3.5, where the $E_{1/2}$ values are plotted vs the Fc/Fc^+ couple. As seen in the figure, the first

two reductions of ($PdCl_2$)LZn and ($PtCl_2$)LZn are the same as first two reductions of [LZn], within experimental error. The addition of one $PtCl_2$ unit to [LZn] shifts the second reduction of the bimetallic complex anodically by 20 mV. The difference between the $PdCl_2$ and $PtCl_2$ complexes is not large and it is not clear that $PtCl_2$ has a greater influence on the second reduction (dianionic form) than does $PdCl_2$. Surprisingly, the third and fourth reductions of ($PdCl_2$)LZn are more difficult than the third and fourth reductions of the parent compound, [LZn]. Contrary to what was seen for the [LZn] derivatives, the binding of $PtCl_2$ and $PdCl_2$ to [LPd] shifts the first reduction anodically by 40 and 50 mV (see Table 3.3), respectively, while for the second reduction $PdCl_2$ shifts anodically by 30 mV compared to the 70 mV in the case of the $PtCl_2$ compound. Like what was seen for [LZn], $PtCl_2$ has a more significant influence on the second reduction. The absolute potential difference between the first and second reductions of [LPd] and [($PdCl_2$)LPd] amounts to 0.35 V while a similar $\Delta E_{1/2}$ of 0.32 V is seen between [LPd] and [($PtCl_2$)LPd], which is one indication that both reductions are macrocycle centered.

As expected, the measured half wave potentials do depend upon the electronic effects of the central metal ion and this is clearly seen by comparisons of $E_{1/2}$ values within a given series of macrocycles where, in each case, the $Mg^{II}(H_2O)$ derivatives are the hardest to reduce and the Pd^{II} compounds are the easiest. This was earlier reported in the series of [LM] compounds where [$LMg(H_2O)$] is reduced to its anion radical form at -0.33 V as compared to -0.26 for the first reduction of [LZn] and [LPd] (see Figure 3.3). Likewise, [$LMg(H_2O)$] is reduced to its dianionic form at -0.70 V in DMSO while [LZn]

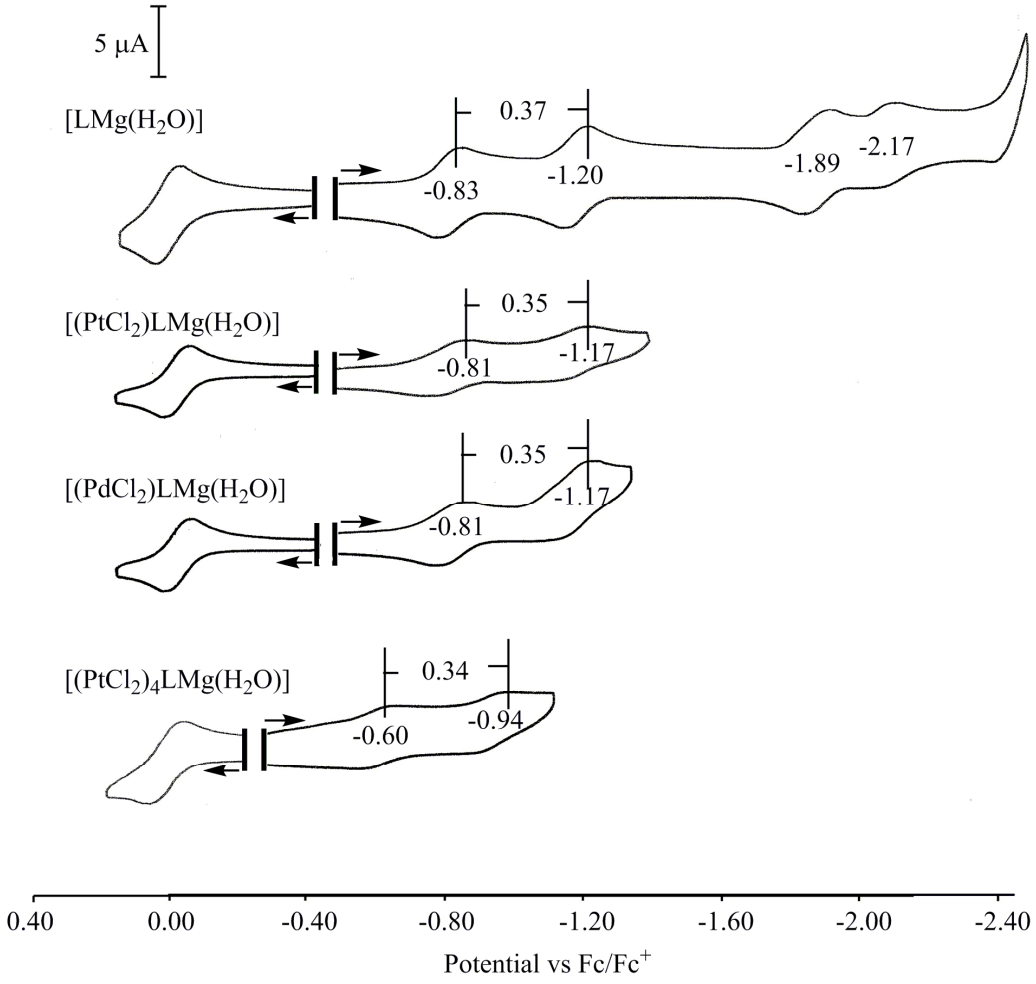

Figure 3.4. Cyclic voltammograms (potential vs. Fc/Fc^+) of [LMg], [$(PtCl_2)$LMg], [$(PdCl_2)$LMg] and [$(PtCl_2)_4$LMg] in DMSO, 0.1 M TBAP. The oxidation potentials of ferrocene is set as 0.00 V.

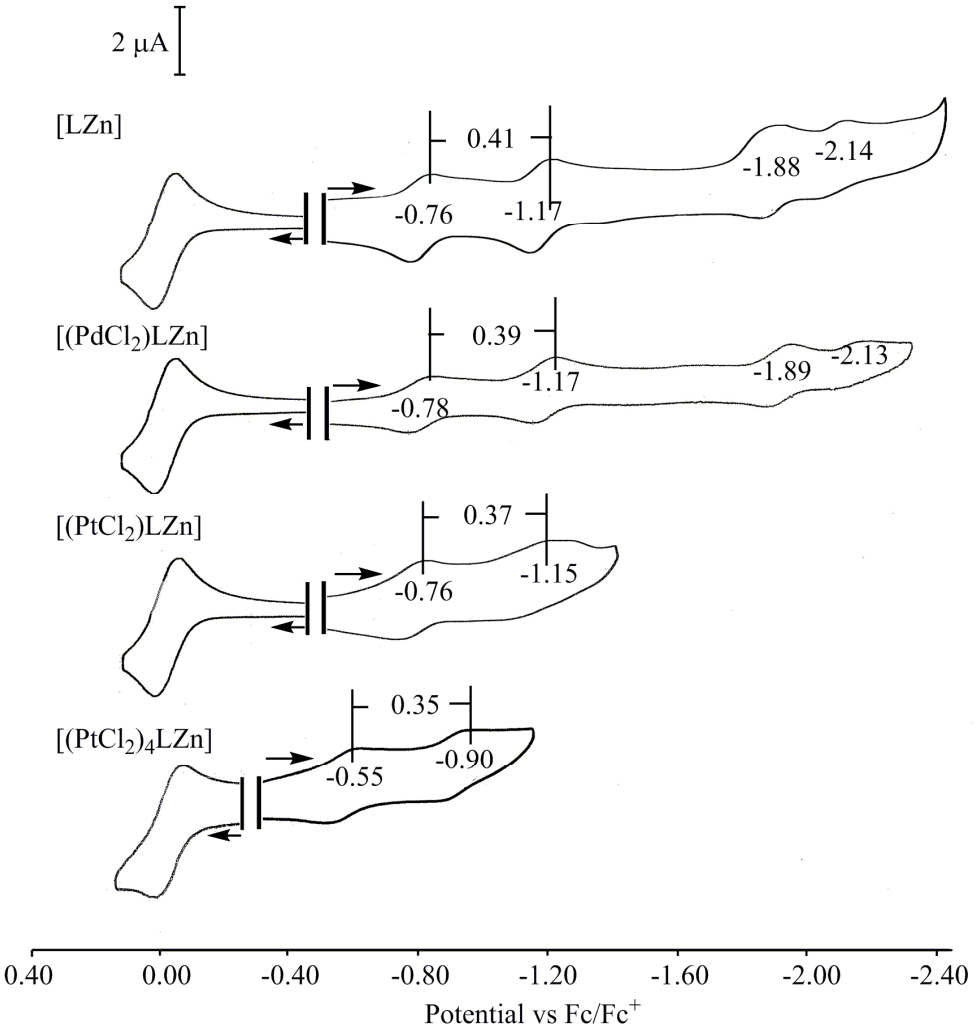

Figure 3.5. Cyclic voltammograms (potential vs. Fc/Fc^+) of [LZn], [$(PdCl_2)$LZn], [$(PtCl_2)$LZn] and [$(PtCl_2)_4$LZn] in DMSO, 0.1 M TBAP. The oxidation potentials of ferrocene is set as 0.00 V.

Table 3.3: Reduction potentials of porphyrazine derivatives in DMSO.

	Reductions vs Fc/Fc^+						
compound	First	Second	Third	Fourth	Fc/Fc^+	ΔE_{1-2}	Ref.
LMg	-0.83	-1.20	-1.89	-2.17	0.50	0.36	13
$LMg(PtCl_2)$	***-0.81***	***-1.17***			0.44	***0.36***	tw
$LMg(PtCl_2)_4$	-0.60	-0.94			0.45	0.34	8
$LMg(PdCl_2)$	***-0.81***	***-1.16***			***0.44***	***0.35***	tw
LZn	-0.76	-1.17	-1.88	-2.14	0.50	0.37	13
$LZn(PtCl_2)$	***-0.76***	***-1.15***			***0.46***	***0.39***	tw
$LZn(PtCl_2)_4$	-0.55	-0.90			0.45	0.35	8
$LZn(PdCl_2)$	***-0.78***	***-1.17***	***-1.89***	***-2.13***	***0.46***	***0.39***	tw
LPd	-0.72	-1.07	-1.69	-2.04	0.46	0.35	15
$LPd(PtCl_2)$	***-0.68***	***-1.00***			***0.44***	***0.32***	tw
$LPd(PtCl_2)_4$	0.46	-0.81			0.46	0.35	8
$LPd(PdCl_2)$	***-0.69***	***-1.04***	***-1.65***	***-1.91***	***0.44***	***0.35***	tw

tw = this work

and [LPd] undergo more facile reductions at $E_{1/2}$ = -0.67 and -0.61 V, respectively. A similar trend in increased ease of reduction is seen for the [($PtCl_2$)LM] derivatives upon going from M = $Mg^{II}(H_2O)$ to Zn^{II} to Pd^{II} and this is illustrated by the three cyclic voltammograms in Figure 3.3.

For the $PdCl_2$ complex, changing the central metal ($Mg(H_2O)$ → Zn → Pd) shifts the 1st reduction potential by 30 mV and 90 mV while shifts of 20 and 130 mV are observed for the pentametallic analogue. Similarily, for the $PtCl_2$ bimetallic complex shifts of 50 and 80 mV going from $Mg(H_2O)$ to Zn and Zn to Pd as the central metal were observed. The exact same shifts are observed for the pentametallic $PtCl_2$ analogues as well.[8]

[($PtCl_2$)(CH_3)$_6$LM]$^{6+}$, [($PdCl_2$)$_4$LM], [($PtCl_2$)$_4$LM] and [(CH_3)$_8$LM]$^{8+}$. As earlier reported in the literature,[8, 15, 16] the addition of four $PtCl_2$ or $PdCl_2$ groups to an [LM] complex leads to significant positive shifts in the reduction potentials. An example of this shift is shown in Figure 3.3 where appending four $PtCl_2$ groups to the macrocycles of [$LMg(H_2O)$] and [LZn] leads to [($PtCl_2$)$_4$$Mg(H_2O)$] and [($PtCl_2$)$_4$Zn] which are reduced in the first one-electron addition at $E_{1/2}$ = -0.15 and -0.10 V, respectively. These $E_{1/2}$ values are 180 and 160 mV easier than half wave potentials for reduction of the parent [LM] complexes. An even larger effect of the four $PtCl_2$ groups is seen on the second reduction potentials of [($PtCl_2$)$_4$$Mg(H_2O)$] and [($PtCl_2$)$_4$Zn] where the positive shift in $E_{1/2}$ amounts to 210 and 220 mV, respectively.

Large positive shifts in $E_{1/2}$ are also seen in the first and second reductions of [($PtCl_2$)(CH_3)$_6$$LMg(H_2O)$]$^{6+}$, [($PtCl_2$)($CH_3$)$_6$LZn]$^{6+}$ and [($PtCl_2$)(CH_3)$_6$LPd]$^{6+}$ as

compared to the parent [LM] compounds with the same central metal ions. This is illustrated in Figure 3.3 and Table 3.3 where half wave potentials for reduction of the three hexacations containing a single externally coordinated $PtCl_2$ group are almost identical to the measured $E_{1/2}$ values for reduction of the uncharged $[(PtCl_2)_4LM]$ derivatives under the same solution conditions.

Furthermore, the $E_{1/2}$ values for reduction of the hexacations are also almost identical to the potentials for reduction of the octacations, $[(CH_3)_8LM)]^{8+}$. For example, $[(PtCl_2)(CH_3)_6LMg(H_2O)]^{6+}$ is reduced at -0.17 and -0.49 V vs SCE in DMSO (see Figure 3.3 and Table 3.3) and exactly the same half wave potentials have been reported for reduction of the octacationic Mg^{II} complex, $[(CH_3)_8LMg(H_2O)]^{8+}$, in DMSO.[13] These two redox potentials are also almost identical to the $E_{1/2}$ values reported for reduction of neutral $[(PtCl_2)_4Mg(H_2O)]$ or $[(PdCl_2)_4Mg(H_2O)]$ in DMSO, thus demonstrating the existance of two groups of electrochemical behavior for the investigated porphyrazines, one for $[LMg(H_2O)]$, $[(PtCl_2)Mg(H_2O)]$ and $[(PdCl_2)Mg(H_2O)]$ and the other for the hexacationic species, the octacationic species and the neutral derivatives containing externally coordinated $PtCl_2$ or $PdCl_2$ units.

In summary, the electrochemical results unequivocally demonstrate that the presence of a single $PtCl_2$ or $PdCl_2$ group on the porphyrazine periphery has little to no effect on the redox potentials as compared to the parent [LM] compound. This contrasts significantly to what occurs upon quaternization and formation of the hexacation which has the same facilitated reductions as the tetrametalated or tetraquaternized species.

3.2.3 Spectroelectrochemistry

The spectroelectrochemical behavior of each metal derivative was investigated under similar solution conditions (higher supporting electrolyte concentration, 0.2 M TBAP) from what was described above for cyclic voltammetry and UV-visible spectral measurements. Examples of UV-visible spectral changes are shown in Figures 3.6 and 3.7 for the first reduction of the neutral and hexacationic Zn^{II} and Mg^{II} derivatives and in Figure 3.8 for the first reduction of $[(PtCl_2)(CH_3)_6LM]^{6+}$, where M = $Mg^{II}(H_2O)$, Zn^{II} and Pd^{II}.

Each series of spectra in Figures 3.6, 3.7, 3.8 are characterized by well defined isobestic points, indicating the lack of a detectable intermediate upon going from the neutral to the singly reduced form of the compound. As described in our previous papers,[8, 13, 15] the first reduction leads to a collapse of the Q-band and the growth of a low-intensity band at 540-572 nm. The singly reduced species are also characterized by broad absorptions at >700 nm. The spectral changes upon the first one-electron reduction are similar for derivatives in each series, independent of the central metal ion, which is an indication that the reductions occur at the macrocycle core.

3.3 Conclusions

The present contribution provides information about the UV-visible spectral behavior and spectroelectrochemical properties of two groups of compounds having the formula $[(M'Cl_2)LM]$ and $[(PtCl_2)(CH_3)_6LM](I)_6$, where L = tetrakis-2,3-[5,6-di(2-pyridyl)pyrazino]porphyrazinato anion, M = Zn^{II}, $Mg^{II}(H_2O)$ or Pd^{II} and M' = Pd^{II} or Pt^{II}. On the basis of the observed spectral and electrochemical behavior we conclude that external monometalation of [LM] to give $[(M'Cl_2)LM]$ leaves the electronic distribution within the macrocycle almost totally unchanged. In contrast, a more significant electronic

perturbation occurs upon formation of the hexacations in the process $[(PtCl_2)LM] \rightarrow [(PtCl_2)(CH_3)_6LM](I)_6$. The electrochemical and spectroscopic data is self-consistent in demonstrating the enhanced electron-withdrawing properties of the $[(CH_3)_6LM]^{6+}$ hexacations. In addition, the spectral and electrochemical behavior of the +6 charged species compares nicely with what has been earlier reported for the full externally metalated or quaternized species, formulated as $[(M'Cl_2)_4LM]$ and $[(CH_3)_8LM](I)_8$, respectively. A comparison of UV-visible spectra for the hexacations in DMSO and in water provides evidence for the three charged compounds being in their pure monomeric form in the nonaqueous solvent and in a monomer/dimer equilibrium in aqueous media. Unfortunately, the low solubility and aggregation of the hexacations in water results in a poor electrochemical response and this limits the obtaining of additional information which might be important for better understanding the use of these materials as photoactive anticancer drugs.

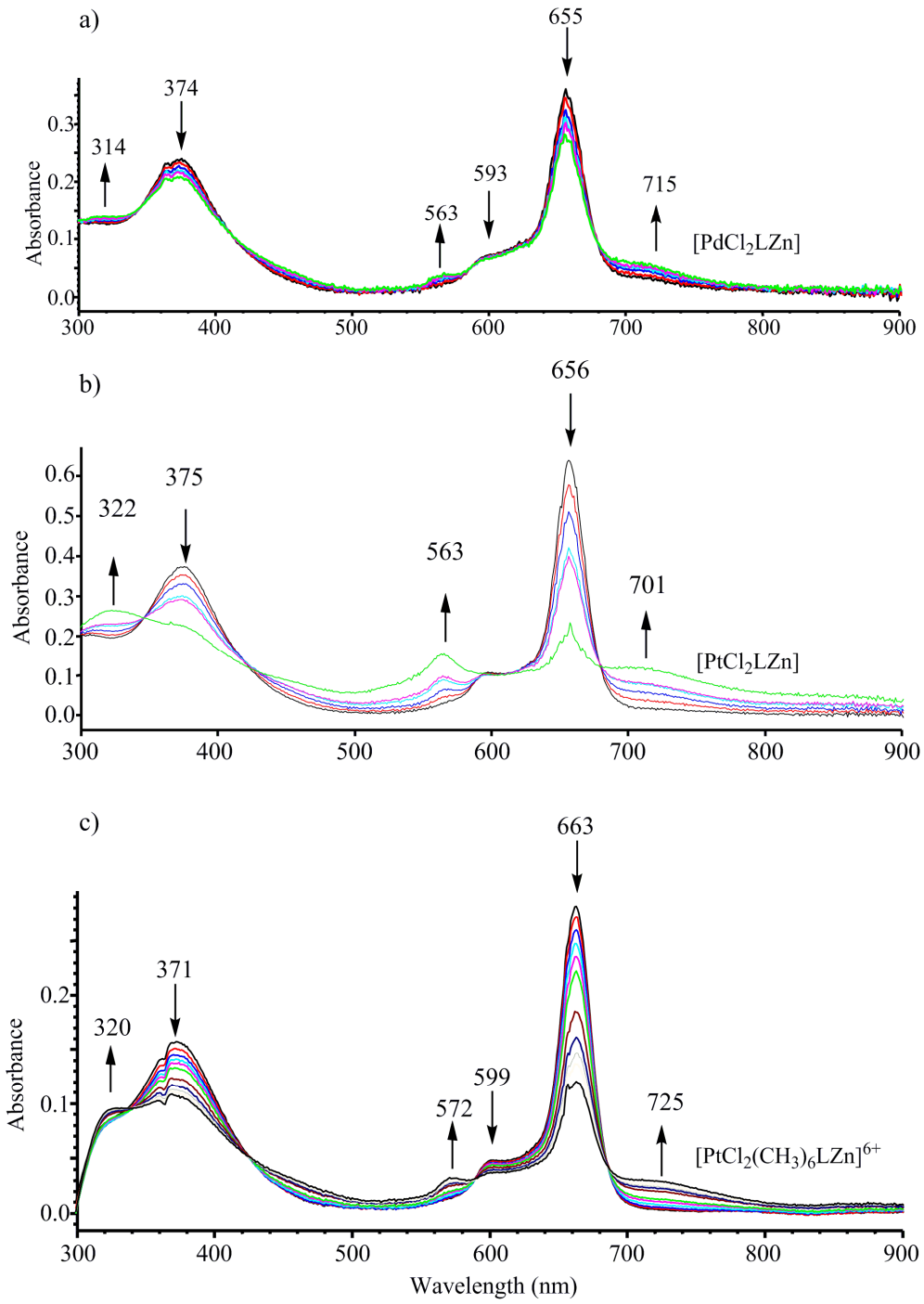

Fig. 3.6. Spectral changes during controlled-potential electrolysis of a) [($PdCl_2$)LZn], b) [($PtCl_2$)L Zn] and c) [($PtCl_2$)(CH_3)$_6$L Zn]$^{6+}$ in DMSO, containing 0.2 M TBAP.

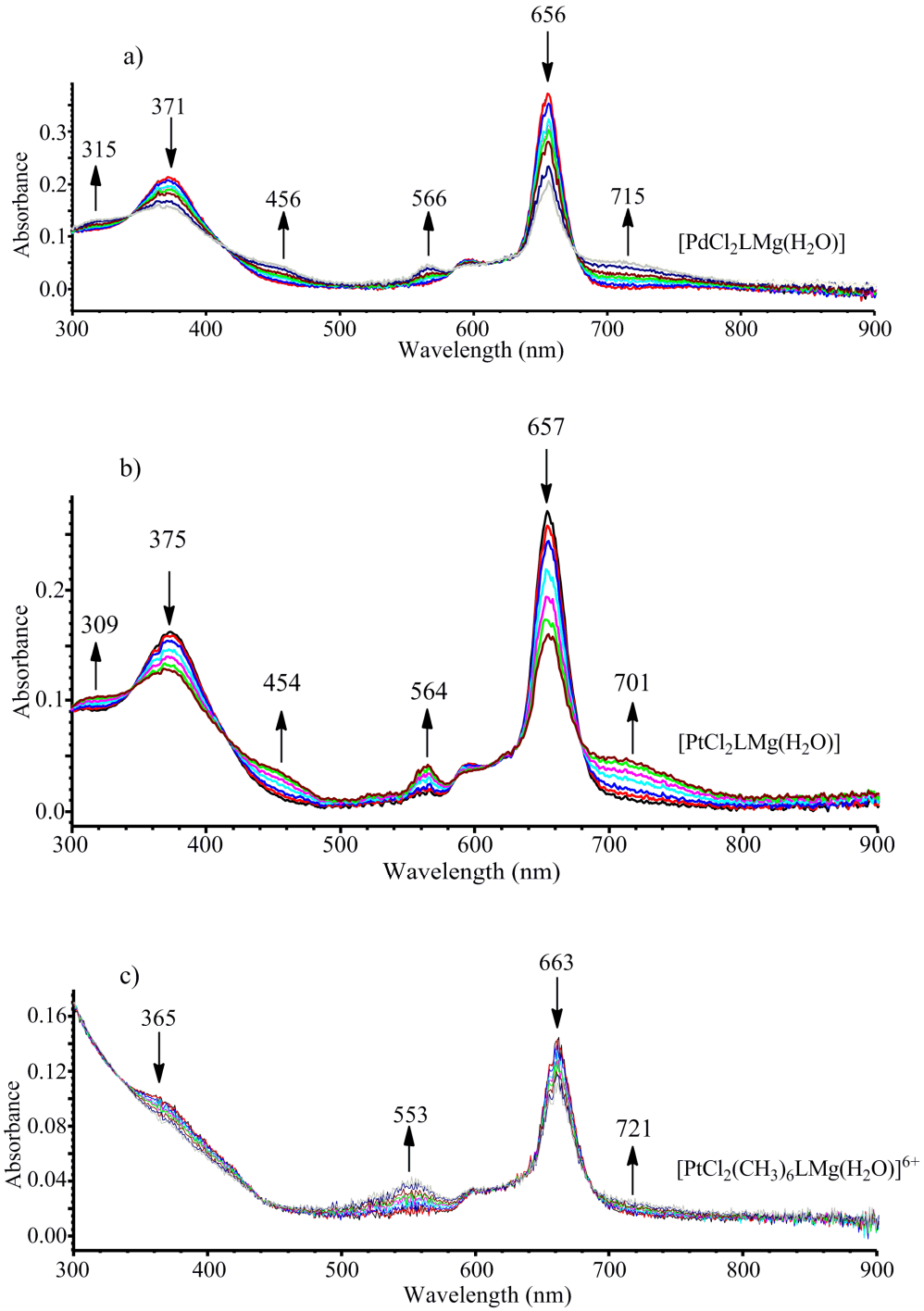

Figure 3.7. Spectral changes during controlled-potential electrolysis of a) $[(PdCl_2)LMg(H_2O)]$, b) $[(PtCl_2)L\ Mg(H_2O)]$ and c) $[(PtCl_2)(CH_3)_6L\ Mg(H_2O)]^{6+}$ in DMSO, containing 0.2 M TBAP.

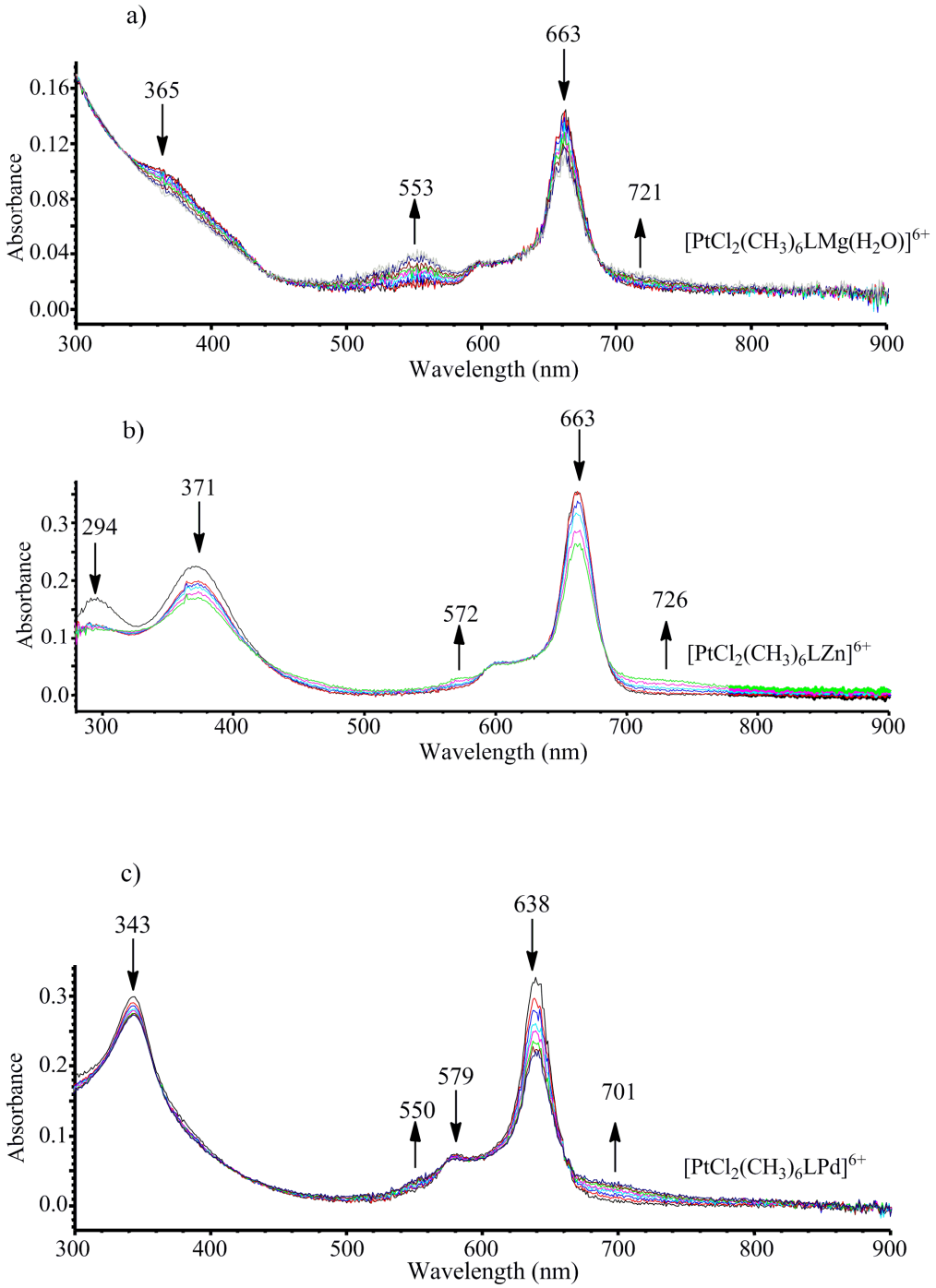

Figure 3.8. Spectral changes during controlled-potential electrolysis of a) $[(PtCl_2)(CH_3)_6LMg(H_2O)]^{6+}$, b) $[(PtCl_2)(CH_3)_6LZn]^{6+}$ and c) $[(PtCl_2)(CH_3)_6LPd]^{6+}$ in DMSO, containing 0.2 M TBAP.

3.5 References

1. Donzello, M. P.; Viola, E.; Bergami, C.; Dini, D.; Ercolani, C.; Giustini, M.; Kadish, K. M.; Meneghetti, M.; Monacelli, F.; Rosa, A.; Ricciardi, G., *Inorg. Chem.* **2008,** *47*, 8757-8766.
2. Donzello, M. P.; Vittori, D.; Viola, E.; Manet, I.; Mannina, L.; Cellai, L.; Monti, S.; Ercolani, C., *Inorg. Chem.* **2011,** *50*, 7391-7402.
3. Celli, J. P.; Spring, B. Q.; Rizvi, I.; Evans, C. L.; Samkoe, K. S.; Verma, S.; Pogue, B. W.; Hasan, T., *Chem. Rev.* **2010,** *110*, 2795-2838.
4. Moreira, L. M.; Viera dos Santos, F.; Pereira Lyon, J.; Maftoum-Costa, M.; Pacheco-Soares, C.; Soares da Silva, N., *Aust. J. Chem.* **2008,** *61*, 741-754.
5. O'Conner, A. E.; Gallagher, W. M.; Byrne, A. T., *Photochem. Photobiol.* **2009,** *85*, 1053.
6. Szacilowski, K.; Macyk, W.; Drzewiecha-Matuszek, A.; Brindell, M.; Stochel, G., *Chem. Rev.* **2005,** *105*, 2647-2694.
7. Castano, A. P.; Mroz, P.; Hamblin, M. R., *Nat. Rev. Cancer* **2006,** *6*, 535-545.
8. Donzello, M. P.; Viola, E.; Ercolani, C.; Fu, Z.; Futur, D.; Kadish, K., *Inorg. Chem.* **2012,** *51*, 12548.
9. Donzello, M. P.; Viola, E.; Mannina, L.; Barteri, M.; Fu, Z.; Ercolani, C., *J. Porphyrins Phthalocyanines* **2011,** *15*, 984-994.
10. Manet, I.; Manoli, F.; Donzello, M. P.; Ercolani, C.; Vittori, D.; Cellai, L.; Masi, A.; Monti, S., *Inorg. Chem.* **2011,** *50*, 7403 - 7411.

11. Manet, I.; Manoli, F.; Donzello, M. P.; Ercolani, C.; Vittori, D.; Cellai, L.; Monti, S., *Org. Biomol. Chem.* **2011,** *9*, 684-688.

12. Manet, I.; Manoli, F.; Donzello, M. P.; Viola, E.; Masi, A.; Andreano, G.; Ricciardi, G.; Rosa, A.; Cellai, L.; Ercolani, C.; Monti, S., *Inorg. Chem.* **2013,** *52*, 321-328.

13. Bergami, C.; Donzello, M. P.; Monacelli, F.; Ercolani, C.; Kadish, K. M., *Inorg. Chem.* **2005,** *44*, 9862-9873.

14. Donzello, M. P.; Ou, Z.; Dini, D.; Meneghetti, M.; Ercolani, C.; Kadish, K. M., *Inorg. Chem.* **2005,** *43*, 8637-8648.

15. Donzello, M. P.; Viola, E.; Cai, X.; Mannina, L.; Rizzoli, C.; Ricciardi, G.; Ercolani, C.; Kadish, K.; Angela, R., *Inorg. Chem.* **2008,** *47*, 3903-3919.

16. Donzello, M. P.; Viola, E.; Cai, X.; Mannina, L.; Ercolani, C.; Kadish, K. M., *Inorg. Chem.* **2010,** *49*, 2447-2456.

17. Kee, H. L.; Bhaumik, J.; Diers, J. R.; Mroz, P.; Hamblin, M. R.; Bocian, D.; Lindsey, J.; Holten, D., *J. Photoch. Photobio. A* **2008,** *200*, 346-355.

18. Edwards, L.; Dolphin, D. H., *J. Mol. Spectrosc.* **1970,** *35*, 90-109.

19. Spellane, P.; Gouterman, M.; Antipas, A.; Kim, S.; Liu, Y. C., *Inorg. Chem.* **1980,** *19*, 386-391.

20. Gouterman, M., In *"The Porphyrins"*, Dolphin, D., Ed. Academic Press: New York, 1978; Vol. III, pp 1-165.

21. Linssen, T. G.; Hanack, M., *Chem. Ber.* **1994,** *127*, 2051-2057.

22. Musil, Z.; Zimcik, P.; Miletin, M.; Kopecky, K.; Lenco, J., *Eur. J. Org. Chem.* **2007,** *2007*, 4535-4542.

23. Sakamoto, K.; Kato, T.; Cook, M. J., *J. Porphyrins Phthalocyanines* **2001,** *5*, 742-750.

24. Kobayashi, N.; Miwa, H.; Nemykin, V. N., *J. Am. Chem. Soc.* **2002,** *124*, 8007.

25. Zimcik, P.; Miletin, M.; Novakova, K.; Kopecky, K.; Dvorakova, Z., *Dyes Pigments* **2009,** *81*, 35-39.

26. Allen, L. C., *J. Am. Chem. Soc.* **1989,** *111*, 9003.

27. Nyokong, T.; Gasyna, Z.; Stillman, M. J., *Inorg. Chem.* **1987,** *26*, 548-553.

28. Donzello, M. P.; Ercolani, C.; Cai, X.; Kadish, K. M.; Ricciardi, G.; Rosa, A., *Inorg. Chem.* **2009,** *48*, 9890-9903.

29. Gritzner, G.; Kuta, J., *Pure Appl. Chem.* **1984,** *56*, 461.

CHAPTER FOUR

UV-Visible and Electrochemical Studies on 2,3-Di(2-pyridyl)-6,7-dicyano-1,4-quinoxaline, $[(CN)_2Py_2Quin]$, Its Complexes $[(CN)_2Py_2QuinMCl_2]$ ($M = Pd^{II}, Pt^{II}$) and Related Compounds

4.1 Introduction. In a previous study,[1] the UV-visible spectral and electrochemical behavior of 2,3-dicyano-5,6-di(2-pyridyl)-1,4-pyrazine, $[(CN)_2Py_2Pyz]$ and 2,3-dicyano-5,6-di(2-thienyl)-1,4-pyrazine, $[(CN)_2Th_2Pyz]$ were reported in nonaqueous solvents (dimethyl sulfoxide, dimethylformamide and pyridine), the examined compounds being known precursors of macrocyclic pyrazinoporphyrazines.[2-11] Similar studies were also carried out on the phenyl analog $[(CN)_2Ph_2Pyz]$, and the two metalated compounds represented as $[(CN)_2Py_2PyzMCl_2]$ (M = Pt^{II}, Pd^{II}). [1] For this series of related compounds, schematically represented in Chart 4.1, it was shown that a one-electron reduction leads, in each case, to formation of the corresponding -1 charged species. The UV-visible spectrum for the anions of $[(CN)_2Py_2Pyz]^{1-}$, $[(CN)_2Th_2Pyz]^{1-}$ and $[(CN)_2Ph_2Pyz]^{1-}$ exhibit peak maxima at 610-630 nm which were assigned as $\pi_1^* \rightarrow \pi_2^*$ transitions.[1] A broad structureless absorption was also observed for electrogenerated $[(CN)_2Py_2PyzPtCl_2]^{1-}$ in the region of 500-900 nm, with the highest intensity band being centered at 705 nm in DMSO and DMF and at 770 nm in pyridine. In the absence of theoretical calculations, these absorptions were tentatively attributed to the presence of $\pi_1^* \rightarrow \pi_2^*$ and MLCT transitions.[1] To the best of our knowledge, there have been no reports in the literature focusing on interpretation of the UV-visible/near IR spectral changes accompanying formation of the one-electron reduced species from the unmetalated or metalated species in Chart 4.1 compounds **4-7** or closely related compounds. This is addressed in the current work, along with the triad of quinoxaline compounds shown in Chart 4.1 (compounds **1-3**), ie. 2,3-di(2-pyridyl)-6,7-dicyano-1,4-quinoxaline, $[(CN)_2Py_2Quin]$, the palladated derivative $[(CN)_2Py_2QuinPdCl_2]$ and the

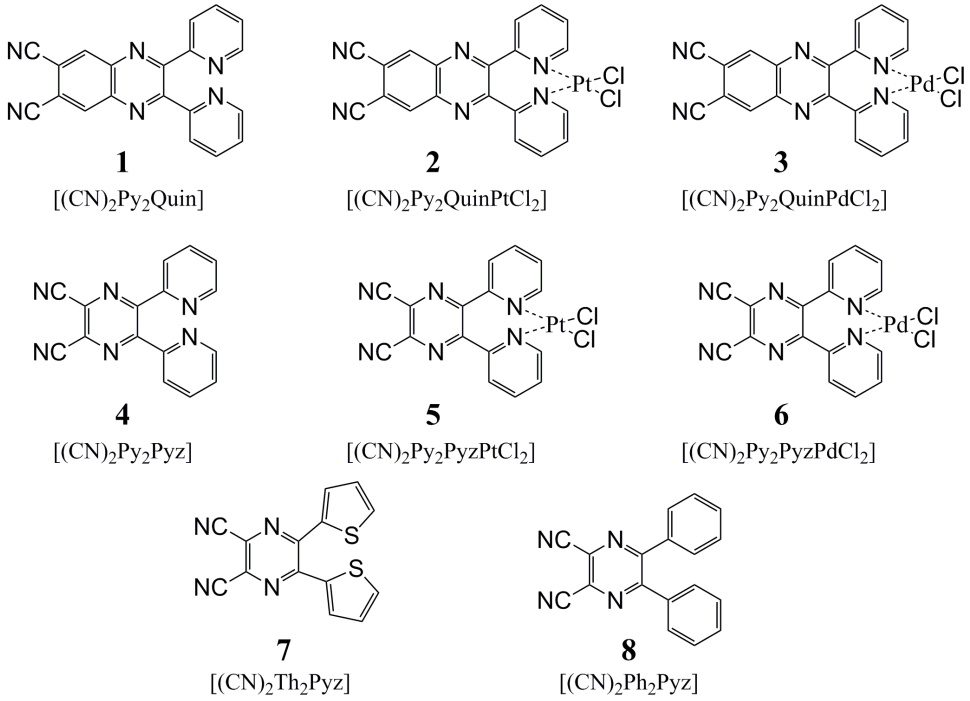

1 [$(CN)_2Py_2Quin$]

2 [$(CN)_2Py_2QuinPtCl_2$]

3 [$(CN)_2Py_2QuinPdCl_2$]

4 [$(CN)_2Py_2Pyz$]

5 [$(CN)_2Py_2PyzPtCl_2$]

6 [$(CN)_2Py_2PyzPdCl_2$]

7 [$(CN)_2Th_2Pyz$]

8 [$(CN)_2Ph_2Pyz$]

Chart 4.1

platinated species [$(CN)_2Py_2QuinPtCl_2$], the latter of which is structurally characterized in the present study. An examination of compounds 1-3 in Chart 4.1 provides parallel information on the site of electron transfer and electronic distribution for compounds 4-8 in Chart 4.1 which carry the dicyanopyrazine fragment. The same two series of compounds were also characterized by Density Functional Theory (DFT) and time-dependent DFT (TDDFT) calculations which provided an explanation of the observed UV-visible spectral features for both the metalated and non-metalated compounds in their neutral and -1 charged forms. The main features of the UV-visible absorption spectra are interpreted in terms of single excitations between the Kohn-Sham frontier orbitals of the gas-phase optimized structures.

4.2 Results and Discussion

4.2.1 Structural Features and ^{1}H and ^{13}C NMR Solution Studies of [$(CN)_2Py_2QuinMCl_2$] (M = Pd^{II}, Pt^{II}).

Before entering the discussion of the electrochemical data, the structural features of the title compounds deserve illustration as to the mode of $PdCl_2$ or $PtCl_2$ coordination to the quinoxaline precursor, [$(CN)_2Py_2Quin$]. Data in the literature indicates that the dipyridinopyrazine moiety can bind metal ions as a bidentate donor, either involving coordination by the two pyridine N atoms on the compound ("py-py" coordination; Scheme 4.1A) or coordination via one pyridine and one pyrazine N atom ("py-pyz" coordination; Scheme 4.1B). Previously published crystallographic data indicate that "py-py" coordination is largely prevalent for metal ions such as Cu^{II}, Ni^{II} or Re^{V}, whereas "py-pyz" coordination is found in the case of Ru^{II}, Co^{II} and Cu^{II}. X-ray structural data

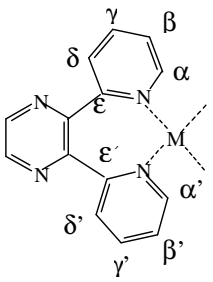

A: “py-py”

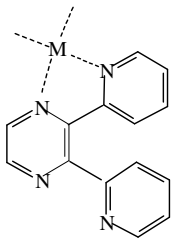

B: “pyz-py”

Scheme 4.1

indicate that a "py-py" type of coordination takes place, in most cases, with Pd^{II} or Pt^{II} metal ions. This includes our earlier characterized $[(CN)_2Py_2PyzMCl_2]$ derivatives (M = Pd^{II}, Pt^{II}; Chart 4.1),[1, 7] the dichloro(6,7-dimethyl-2,3-di(2-pyridyl)quinoxaline)palladium(II) complex[12] and two related quinoxaline species with Pt^{II}, ie. dichloro(2,3-di(2- pyridyl)quinoxaline)platinum(II)[13] and dichloro(6,7-dimethyl-2,3-di(2-pyridyl)quinoxaline)platinum(II).[12] No unequivocal "py-pyz" type of coordination has so far been established by X-ray studies. Nevertheless, NMR spectral data demonstrate the occurrence of a "py-pyz" coordination for $[(dpq)PtCl_2]$ (dpq = 2,3-di-2-pyridyl-5,6-dihydropyrazine)[12] and $[TPyPyz(PtCl_2)_2]$ (TPyPyz = 2,3,5,6-tetra(2-pyridyl)pyrazine).[14]

In the case of the currently studied title compounds, the Pd^{II} derivative $[(CN)_2Py_2QuinPdCl_2]$ was established to exhibit py-py coordination by single-crystal X-ray analysis.[15] This mode of binding is also seen for the isostructural Pt^{II} analog, which coordinates solvent molecules in a stoichiometric molar ratio of 1:1 and is correctly formulated as $[(CN)_2Py_2QuinPtCl_2]\cdot CH_3CN$. An ORTEP view of the Pt^{II} complex is shown in Figure 4.1.[16] The quasi-planar coordination site $N_{2(py)}PtCl_2$ is oriented almost perpendicular to the plane of the quinoxaline fragment and the two pyridine rings in each coordination site are nearly orthogonal to each other. This type of arrangement closely resembles what is observed for complexes of the formula $[(CN)_2Py_2PyzMCl_2]$ (M = Pd^{II}, Pt^{II}; Chart 4.1).[1, 7]

The NMR spectra of the triad $[(CN)_2Py_2Quin]$, $[(CN)_2Py_2QuinPdCl_2]$ and $[(CN)_2Py_2QuinPtCl_2]$ obtained in DMSO-d_6 are shown in Figure 4.2. The ^1H and ^{13}C

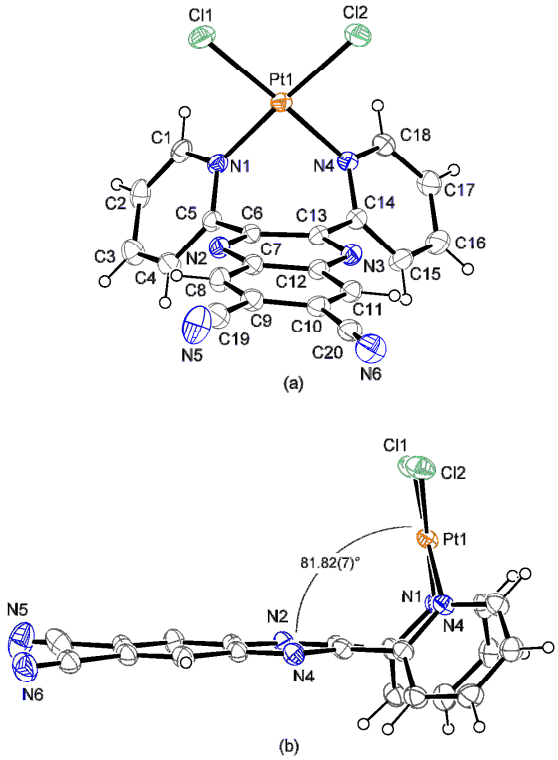

Figure 4.1. ORTEP front (top) and side (bottom) views (30% probability ellipsoids) of $[(CN)_2Py_2QuinPtCl_2]$.

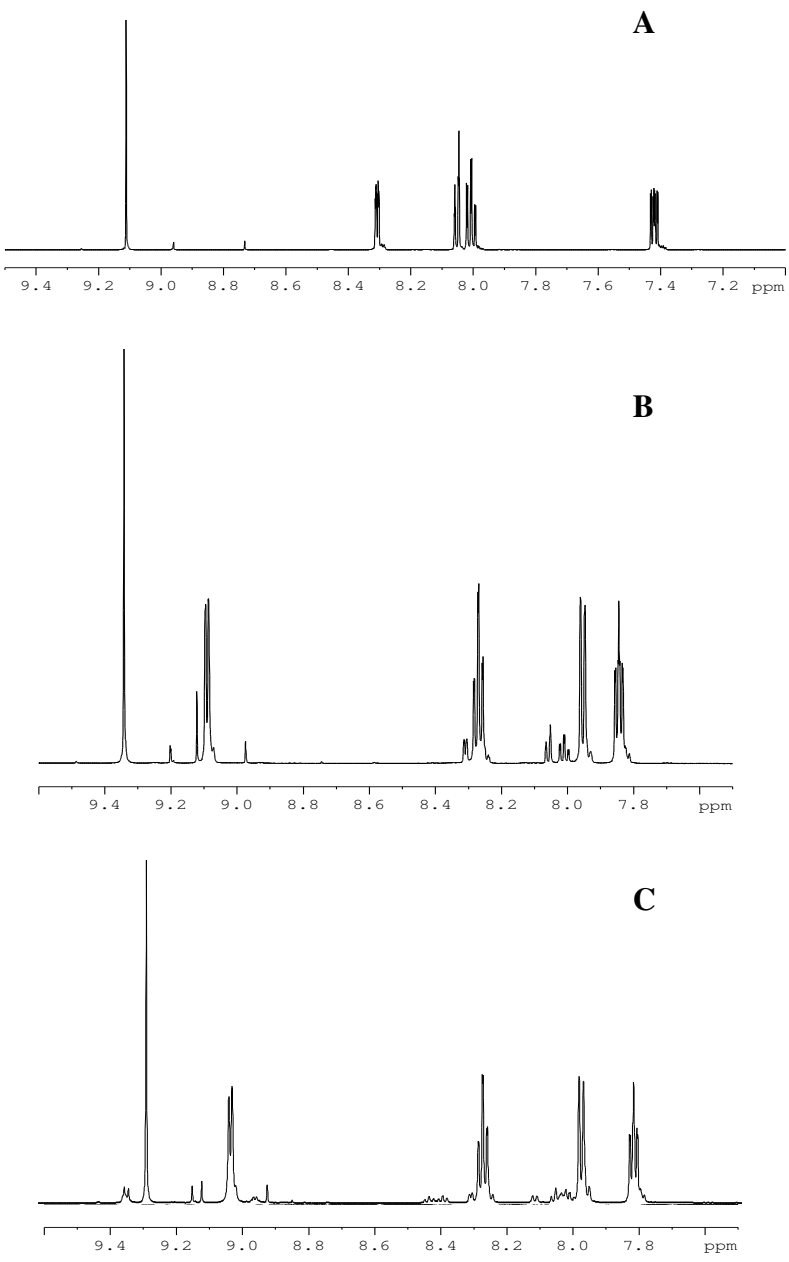

Figure 4.2. ^{1}H NMR spectra in DMSO-d_6 at 300 K of A) $[(CN)_2Py_2Quin]$, B) $[(CN)_2Py_2QuinPdCl_2]$ and C) $[(CN)_2Py_2QuinPtCl_2]$.

Table 4.1. ^{1}H and ^{13}C NMR Assignments of $[(CN)_2Py_2Quin]$, $[(CN)_2Py_2QuinPdCl_2]$ and $[(CN)_2Py_2QuinPtCl_2]$ in DMSO-d_6 at 300 K.

	$[(CN)_2Py_2Quin]$				**$[(CN)_2Py_2QuinPdCl_2]$**				**$[(CN)_2Py_2QuinPtCl_2]$**			
	^{1}H	**m**	***J* (Hz)**	**^{13}C**	**^{1}H**	**m**	***J* (Hz)**	**^{13}C**	**^{1}H**	**m**	***J* (Hz)**	**^{13}C**
α[a]	8.307	ddd	4.8, 1.7, 1.0	149.0	9.080	bd	5.8	153.3	9.033	d	5.6	154.1
β[a]	7.420	ddd	4.8, 7.6, 1.3	122.7	7.843	ddd	5.8, 7.7, 1.3	128.0	7.813	ddd	5.6, 7.7, 1.3	128.6
γ[a]	8.006	ddd	7.6, 7.6, 1.7	137.7	8.269	ddd	7.7, 7.9, 1.3	141.5	8.269	ddd	7.7, 7.7, 1.3	141.2
δ[a]	8.052	ddd	7.6, 1.0, 1.0	124.8	7.954	ddd	7.9, 0.9, 0.9	129.5	7.972	d	7.7	129.6
CH, CH	9.110	s		137.84	9.350	s			9.287	s		137.5

[a] See Scheme 4.1A

NMR spectral data for the Pd^{II} complex (Table 4.1) are in substantial agreement with results previously reported for the same compound in the same solvent,[15] thus indicating that the earlier described experimental conditions and new conditions used in the present study for synthesis of the palladated derivative lead to exactly the same final product in both cases.

The set of four resonance peaks observed in the ^1H NMR spectra of the three quinoxaline compounds in DMSO-d_6 (Figure 4.2 and Table 4.1) indicates an equivalence of the two pyridine rings. This is in agreement with expectation for the unmetalated species and strongly suggests a "py-py" coordination, as was established for the Pd^{II} and Pt^{II} derivatives by X-ray work. From the chemical shifts in Table 4.1, it is evident that the binding of $PdCl_2$ or $PtCl_2$ to $[(CN)_2Py_2Quin]$ leads to a low-field shift of resonance peaks for the α-, β-, and γ-type H atoms (see labelling in Scheme 4.1). A fourth resonance peak (δ H atom) shows only a small change in the reverse direction upon $PdCl_2$ or $PtCl_2$ coordination. As might be expected, the highest shift is observed for the α proton, which is the one closest to the coordinated N atom. These results fully coincide with the NMR spectral data obtained in DMF-d_7 for the parallel series of examined compounds, $[(CN)_2Py_2Pyz]$ and $[(CN)_2Py_2PyzMCl_2]$ (M = Pd^{II}, Pt^{II}).[1, 7]

4.2.2 Electrochemical and Spectroelectrochemical Measurements.

Cyclic voltammograms illustrating the reductions of $[(CN)_2Py_2Quin]$ in three nonaqueous solvents are shown in Figure 4.3 and a summary of the half-wave potentials are given in Table 4.2. On scanning the potential from 0.0 to -2.0 V, two reversible reductions are observed at $E_{1/2}$ = -0.88 to -0.97 V for the first process and $E_{1/2}$ = -1.58 to -1.71 V for

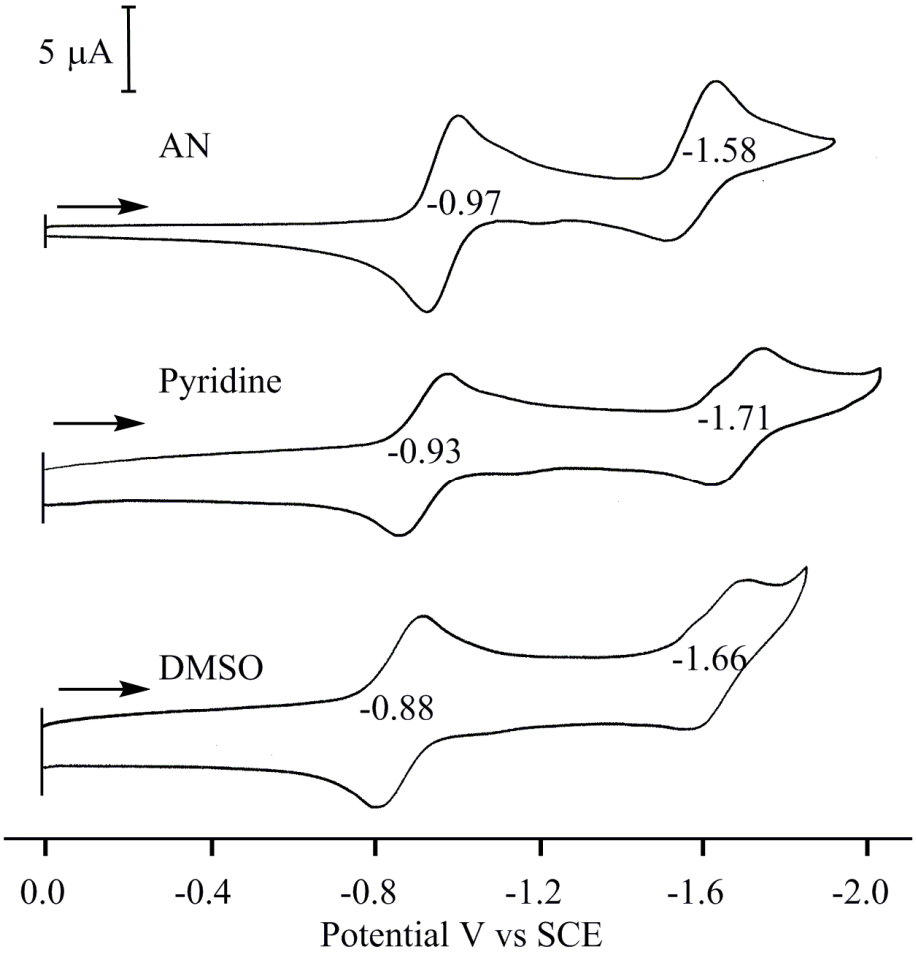

Figure 4.3: Cyclic voltammograms of $[(CN)_2Py_2Quin]$ in AN, Pyridine, and DMSO, containing 0.1 M TBAP. Scan rate 0.1 Vs^{-1}.

Table 4.2: Reduction potentials of $[(CN)_2Py_2Quin]$, $[(CN)_2Py_2QuinPdCl_2]$, $[(CN)_2Py_2QuinPtCl_2]$ and Related Compounds in DMSO, AN, and Pyridine containing 0.1 M TBAP. Scan rate 0.1 Vs^{-1}.

		$E_{1/2}$, V vs SCE			
Compound	Solvent	1st red	[a]	2nd red	ref
$[(CN)_2Py_2Quin]$	DMSO	-0.88		-1.66	tw
$[(CN)_2Py_2QuinPdCl_2]$	DMSO	-0.58[b]	0.34		tw
$[(CN)_2Py_2QuinPtCl_2]$	DMSO	-0.63	0.25	-1.37	tw
$[(CN)_2Py_2Pyz]$	DMSO	-0.87		-1.72[b]	1
$[(CN)_2Py_2PyzPdCl_2]$	DMSO	-0.54[b]	0.33		1
$[(CN)_2Py_2PyzPtCl_2]$	DMSO	-0.60	0.27	-1.25	1
$[(CN)_2Ph_2Pyz]$	DMSO	-0.98		-1.83[b]	tw
$[(CN)_2Th_2Pyz]$	DMSO	-0.87			tw
$[(CN)_2Py_2Quin]$	AN	-0.97		-1.58	tw
$[(CN)_2Py_2QuinPdCl_2]$	AN	-0.62[b]	0.35		tw
$[(CN)_2Py_2QuinPtCl_2]$	AN	-0.70	0.27	-1.43	tw
$[(CN)_2Py_2Pyz]$	AN	-1.01			tw
$[(CN)_2Ph_2Pyz]$	AN	-1.12		-1.92[b]	tw
$[(CN)_2Th_2Pyz]$	AN	-1.01		-1.84[b]	tw
$[(CN)_2Py_2Quin]$	Pyridine	-0.93		-1.71	tw
$[(CN)_2Py_2QuinPdCl_2]$	Pyridine	-0.92		-1.65	tw
$[(CN)_2Py_2QuinPtCl_2]$	Pyridine	-0.65	0.28	-1.41	tw
$[(CN)_2Py_2Pyz]$	Pyridine	-0.93		1.80[b]	1
$[(CN)_2Py_2PyzPtCl_2]$	Pyridine	-0.62	0.31	1.29	1
$[(CN)_2Ph_2Pyz]$	Pyridine	-1.05		-1.92[b]	1
$[(CN)_2Th_2Pyz]$	Pyridine	-0.93		-1.82[b]	1

[a]Difference in potentials between $E_{1/2}$ or E_p for first reductions and that of the parent compound $[(CN)_2Py_2Quin]$ or $[(CN)_2Py_2Pyz]$. [b]Denotes peak potential.

the second process, at a scan rate of 0.1 Vs^{-1}. Cathodic peak currents for the two reductions are similar to each other in each solvent and involve stepwise one-electron additions as described by equations 4.1 and 4.2.

$$[(CN)_2Py_2Quin] + e^- \rightleftharpoons [(CN)_2Py_2Quin]^{\bullet -} \quad (4.1)$$

$$[(CN)_2Py_2Quin]^{\bullet -} + e^- \rightleftharpoons [(CN)_2Py_2Quin]^{2-} \quad (4.2)$$

Coincidently, the first reduction of compound **1** corresponds to the first reduction of $[(CN)_2Py_2Pyz]$ (compound **4**) (structure shown in Chart 4.1), whose potential ranges from -0.87 to -1.01V (vs SCE) in DMSO, Pyridine, and AN as seen in Table 4.2. Expansion of the conjugated system by a benzene ring appears to stabilize the second reduction, which is reversible, as seen in Figure 4.3, unlike the second reduction of compound **4**.[1]

In AN, two reversible processes are observed at -0.97 V and -1.58 V. Comparatively, in DMSO the first reduction is easier by 90 mV but the second reduction on the other hand is harder by 80 mV. On the reverse scan, there is a peak around -1.20 V and upon reversal a corresponding cathodic peak is observed. Similar behavior is also observed for the analogous pyrazine derivative in various solvents.[1] This process was identified as the product of a chemical reaction following the second reduction by Cai et al.[1] but the product was not identified.

Very similar reduction potentials are also observed for the first (reversible) and second (irreversible) reduction of the analogs bearing thienyl and phenyl substituents, ie. $[(CN)_2Th_2Pyz]$ and $[(CN)_2Ph_2Pyz]$ (see Table 4.2). This result suggests that the redox behavior of the examined compounds is preponderantly determined by the

dicyanoquinoxaline or dicyanopyrazine fragments, with a negligible influence of the residual substituents opposite the dicyano groups on the pyrazine ring.

The electrogenerated [$(CN)_2Py_2Quin$] (compound **1**) monoanion is stable on the electrochemical and spectroelectrochemical time scales and the UV-visible spectral changes observed as a function of time can be seen in Figure 4.4. The neutral spectra of compound **1** show absorption peaks at 284 and 355 nm in DMSO and 283 and 351 nm in AN. Its pyrazino counterpart, [$(CN)_2Py_2Pyz$], shows a similar absorption at 314 nm in DMSO and was assigned as a π-π^* transition.[1] The lower energy absorption have been previously assigned to a n-π^* transition for quinoxaline and the remaining band to a π-π^* absorption.[17] Halverson et al.[18] also assigned similar transitions for pyrazine making the 314 nm absorption previously mentioned a n-π^* transition since the π-π^* transition could not be observed using a glass thin-layer cell.

In DMSO, new peaks arise at 277, 337, 420, 585, 641, and 700 nm upon applying a potential negative of the first reduction. The peak separations, of the new peaks at wavelengths longer than 550 nm, are 56 and 59 nm. Cai et al.[1] showed for the related pyrazine compound that there is a decrease in absorption of the neutral peak at 314 nm after reduction and an increased absorption of two new peaks at the longer wavelengths of 390 and 610 nm, in DMSO. The formation of three new absorptions for compound **1** centered around 641 nm compared to the peak at 610 nm for compound **4** may be due to degenerate sites not available to the pyrazine derivative due to a smaller π system. Spectral changes for the first reduction of compound **1** in DMSO and AN are similar with three new peaks growing between 582 nm and 707 nm, as seen in Figure 4.4.

Figure 4.5 shows the cyclic voltammograms of compound **2** in Pyridine, DMSO, and AN. Two reversible one-electron reductions are obtained in each solvent. Both reductions are more facile in DMSO ($E_{1/2}$ = -0.63 and -1.37 V) by 20 and 40 mV in pyridine and 70 and 50 mV in AN. The potential difference between the first and second reduction decreases by 20 mV going from pyridine (0.76 V) to DMSO (0.74 V) and finally to AN (0.72 V).

Noteworthy, both first and second processes occur at $E_{1/2}$ values 250 and 290 mV less negative than those of [$(CN)_2Py_2Quin$] (compound **1**), in DMSO. This means that electron uptake for both processes is facilitated in the platinated species as a result of the electron withdrawing effect caused by Pt^{II} coordination. As can be seen from the data listed in Table 4.2, this behavior nicely parallels that observed in DMSO (and in pyridine and DMF as well) for the couple of analogs [$(CN)_2Py_2Pyz$] and [$(CN)_2Py_2PyzPtCl_2$] in terms of the measured absolute potential values and their change in the two redox processes when going from the unmetalated to the metalated species (second redox process for [$(CN)_2Py_2Pyz$] disturbed by an EC mechanism and only the E_{pc} value could be defined).[1]

Similar shifts are also seen in pyridine with shifts in the first reduction by 280 mV and the second by 300 mV. In AN, the first reduction shift by 250 mV but the second reduction is only easier by 160 mV, which is half of what is seen in DMSO and Pyridine under similar solution conditions. These results also correspond to the trend seen for adding $PtCl_2$ to compound **4**. In DMSO and pyridine, the first reduction of compound **5** is easier than compound **4** by 0.27 to 0.31 V.[1] This indicates similar reduction mechanisms

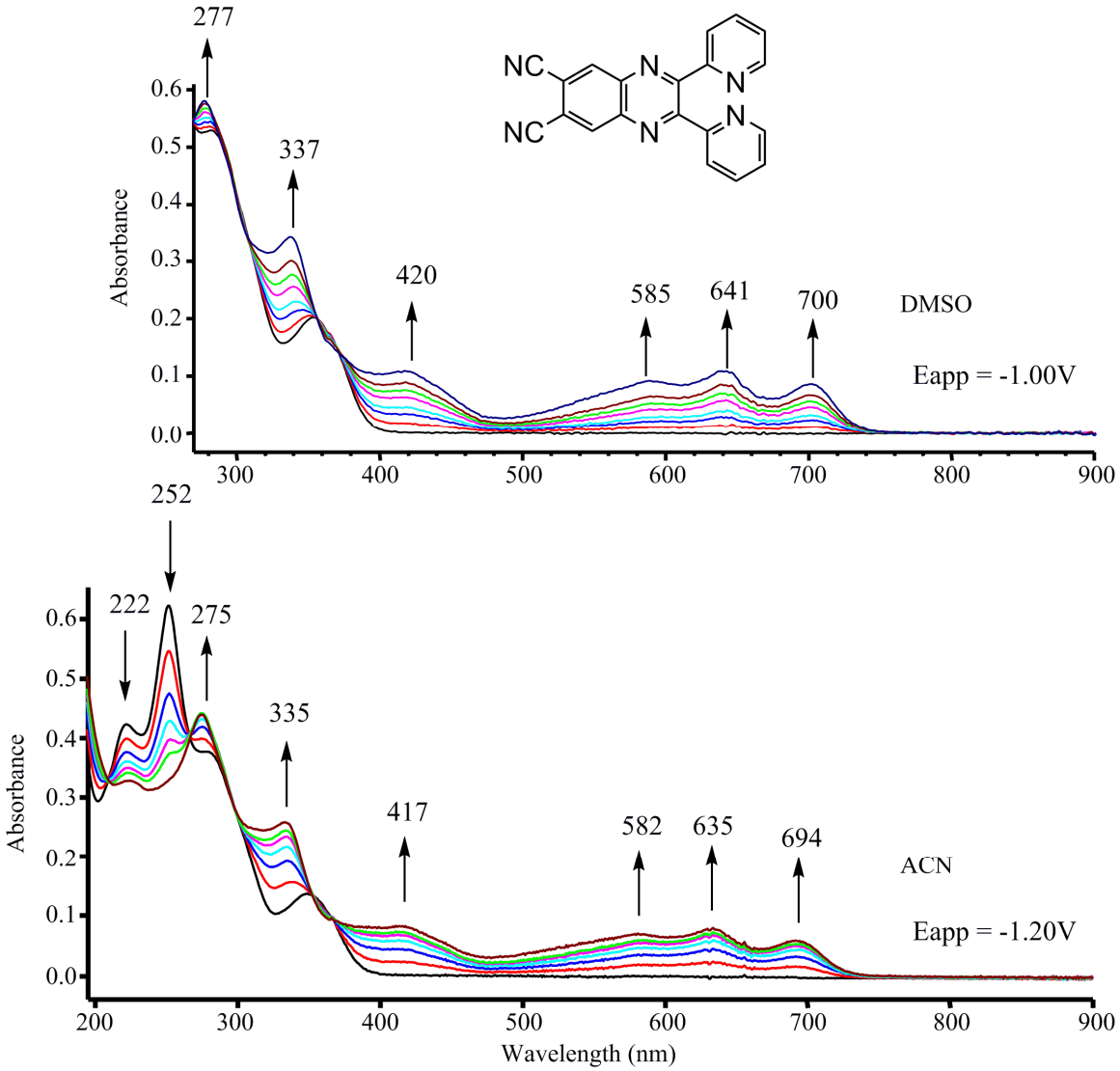

Figure 4.4: Spectral changes of the first reduction of $[(CN)_2Py_2Quin]$ in DMSO and AN, containing 0.2 M TBAP.

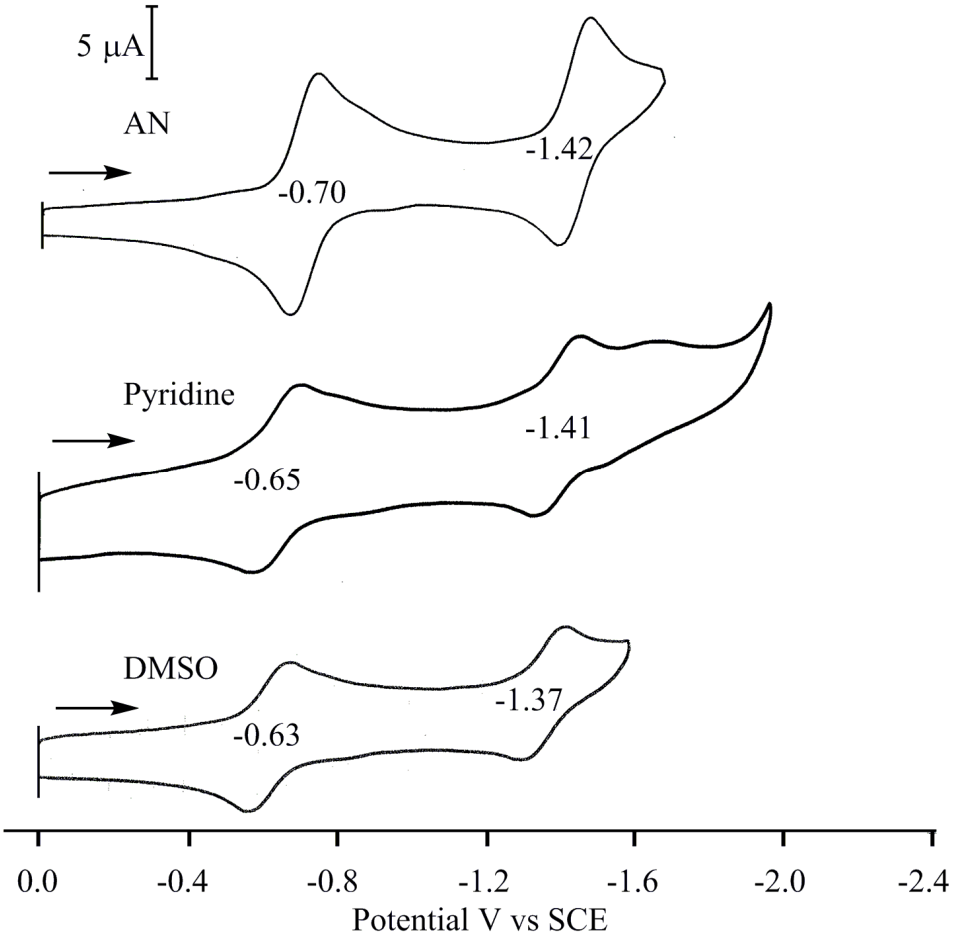

Figure 4.5: Cyclic voltammogram of $[(CN)_2Py_2QuinPtCl_2]$ in AN, Pyridine, and DMSO, containing 0.1 M TBAP, scan rate 0.1 Vs^{-1}.

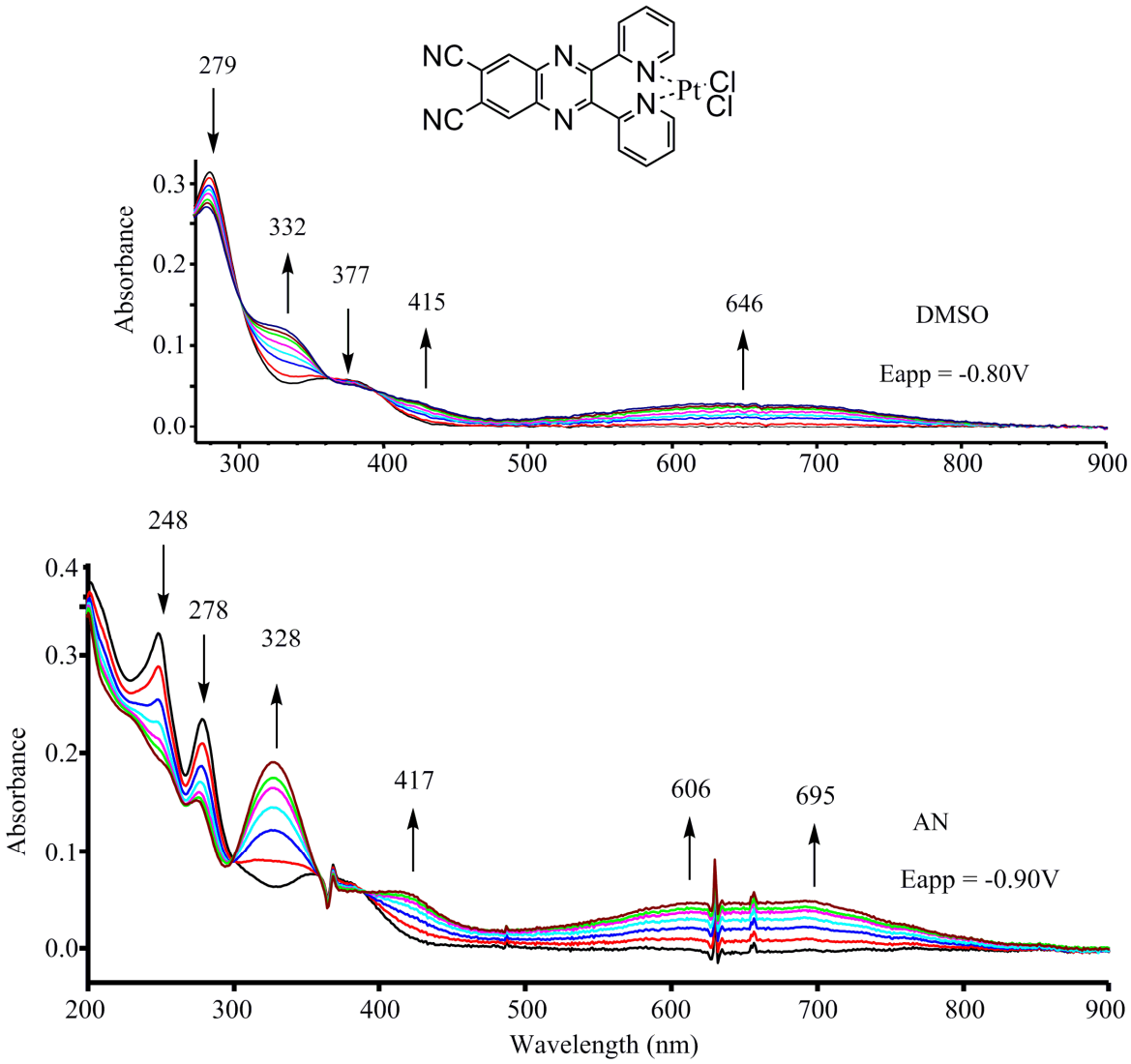

Figure 4.6: Spectral changes of the first reduction of $[(CN)_2Py_2QuinPtCl_2]$ (Compound **2**) in DMSO and AN, containing 0.2M TBAP.

which are described by equations 4.3 and 4.4:

$$[(CN)_2Py_2QuinPtCl_2] + e^- \rightleftharpoons [(CN)_2Py_2QuinPtCl_2]^{\bullet -} \quad (4.3)$$

$$[CN)_2Py_2QuinPtCl_2]^{\bullet -} + e^- \rightleftharpoons [(CN)_2Py_2QuinPtCl_2]^{2-} \quad (4.4)$$

Like the parent unmetallated compound, UV-visible spectra were taken after each one-electron reduction of compound **2**, in a quartz thin-layer cell, as a function of time in DMSO and AN (see Figure 4.6).

The first reduction is spectrally reversible in both solvents and similar spectra are obtained for the electrogenerated monoanion. Absorptions of the neutral compound are seen at 278-279 nm for the π-π* transitions and 368-379 nm for the n-π* transitions, which are blue-shifted and bathochromically shifted with respect to the unmetallated precursor. Upon reduction, there is a decrease in the neutral absorption intensities and the formation of new peaks at 415-417nm, 328-332nm, and a broad peak below 600nm in both DMSO and AN.

The first reduction of $[(CN)_2Py_2QuinPdCl_2]$ is irreversible in DMSO (Figure 4.7) and located at *E*p= -0.58 V for a scan rate of 0.1 Vs^{-1}. This peak potential is positively shifted by 300 mV, as compared to the reversible $E_{1/2}$ value measured for the first reduction of the parent compound $[(CN)_2Py_2Quin]$, closely recalling results for the corresponding platinated species. Thus, for both the $PtCl_2$ and $PdCl_2$ derivatives, there is a comparable positive shift of potential due to the electron withdrawing effect of the coordinated metal center. The similarity in the first reduction potentials of $[(CN)_2Py_2QuinPdCl_2]$ and $[(CN)_2Py_2QuinPtCl_2]$ are consistent with the conjugated π-ring system of the quinoxaline moiety being the site of electron transfer in both compounds.

The global reduction process observed by cyclic voltammetry in DMSO for the quinoxaline palladated species [(CN)2Py2QxPdCl2] (Figure 4.7) closely recalls the parallel ECEC mechanism earlier reported for the Pd^{II} pyrazine analog $[(CN)_2Py2PyzPdCl_2]$,1 a process which implies an initial reduction of Pd^{II} to Pd^{I} and/or Pd^0 prior to reduction at the organic part of the molecule. For the currently studied palladated species, the irreversible first reduction at Ep = -0.58 V is assigned as a conversion of $[(CN)_2Py_2QuinPdCl_2]$ to the -1 charged species, $[(CN)_2Py_2QuinPdCl_2]^{1-}$ (see Scheme 4.2), after which a fast chemical reaction is proposed to occur where an electron is transferred from the reduced organic moiety to Pd^{II}, giving Pd^{I}. The process at -0.87 V most likely involves a $Pd^{I} \rightarrow Pd^0$ process with the concomitant release of the metal and Cl^- ions, followed by first reduction of the just formed neutral unmetalated species $[(CN)_2Py_2Quin]$. The second reduction is at -1.59 V. Noteworthy, the closely lying potentials for reduction of Pd^{I} to Pd^0 and the first reduction of $[(CN)_2Py_2Quin]$ to $[(CN)_2Py_2Quin]^{1-}$ are distinct and positioned at -0.82 and -0.97 V in AN (Figure 4.7). Moreover, two distinct processes are also found in DMSO for the pyrazine analog $[(CN)_2Py_2PyzPdCl_2]$ at -0.78 (E_p) and -0.88 V ($E_{1/2}$).[1] $PdCl_2$ dissociates immediately from the $[(CN)_2Py_2QuinPdCl_2]$ complex as seen by the voltammogram in Figure 4.7 which closely resembles what is observed for $[(CN)_2Py_2Quin]$ in pyridine (Figure 4.3). A loss of coordinated $PdCl_2$ was also reported to occur for the pyrazine analog $[(CN)_2Py_2QuinPdCl_2]$ (compound **6**) and the related pentapalladated porphyrazine complex $[(PdCl_2)_4LM]$ discussed in the previous chapter.[1, 7]

Additional evidence for the mechanism shown in Scheme 4.2 is given by UV-vis

spectra measured during controlled potential reduction of the compound in a thin layer cell at an applied potential of -0.65 V (Figure 4.8). The lack of observed spectral changes assigned to reduction of the organic moiety is consistent with an initial reduction of the Pd^{II} metal ion to its Pd^{I} form. The further controlled potential reduction of $[(CN)_2Py_2QuinPdCl_2]$ at *E*app = -1.0 V in DMSO (Figure 4.9) would then generate Pd0 and the related neutral compound $[(CN)_2Py_2Quin]$, the latter of which is reduced to its mono-anionic form at $E_{1/2}$ = - 0.87 V. One justification for this assignment is given by the fact that the final spectrum in Figure 4.9, after reduction at E_{app} = -0.98 V, is almost identical to the spectrum of $[(CN)_2Py_2Quin]^{1-}$ which was electrogenerated from $[(CN)_2Py_2Quin]$ in the absence of $PdCl_2$ (Figure 4.8), thus adding further support for the proposed mechanism in DMSO. Similar to what is observed for the platinated quinoxaline species, the first reduction of the Pd^{II} analog $[(CN)_2Py_2QuinPdCl_2]$ occurs at a potential of -0.58 V, which is 300 mV less negative than for reduction of the unmetalated species. This reinforces the proposal that metalation at the pyridine rings makes the complexes more easily reducible due to the electron withdrawing effect of the metal centre.

Appending both groups to compound **1** make the first reduction easier by more than 0.25V in DMSO and AN and is an indication of a similar site of electron transfer in both molecules. Thus we assign the reduction to the conjugated π system. As seen with related palladated precursors and macrocycles,[1, 6, 7] $PdCl_2$ is reduced and removed from the parent complex after the first reduction. Spectral changes asscociated with this process in DMSO are a decrease in the absorption at 280 nm without the formation of any

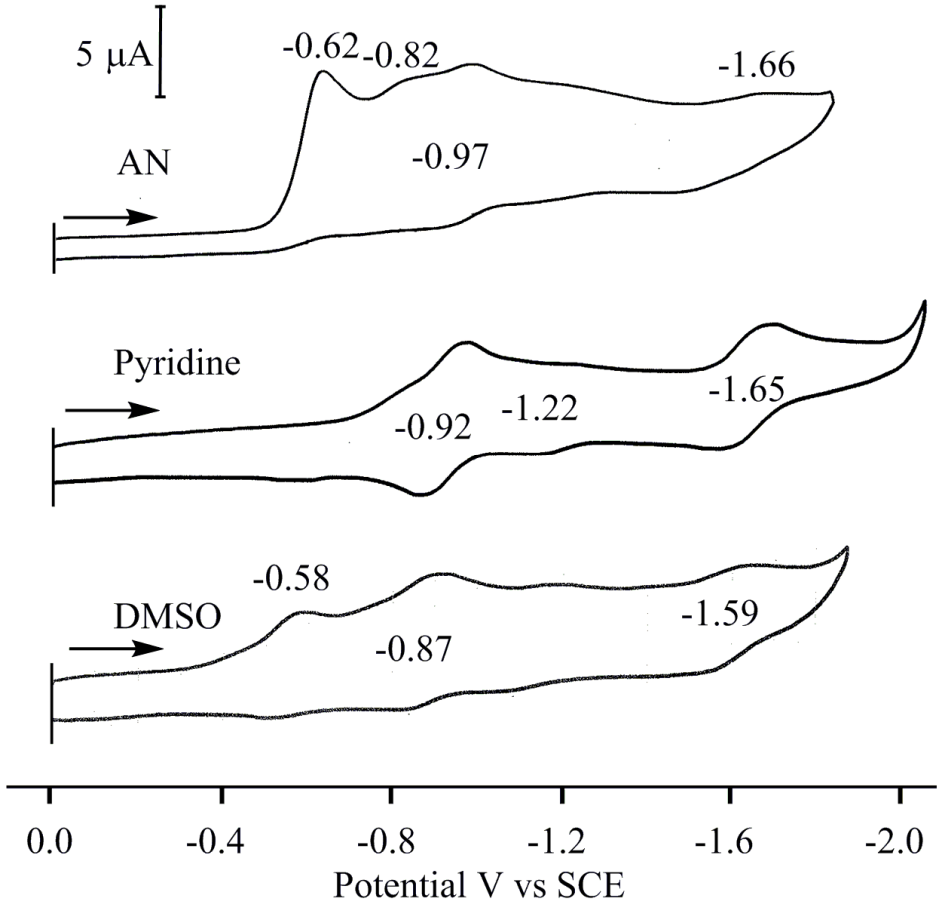

Figure 4.7: Cyclic voltammogram of $[(CN)_2Py_2QuinPdCl_2]$ in AN, Pyridine, and DMSO, containing 0.1 M TBAP, scan rate 0.1 Vs^{-1}.

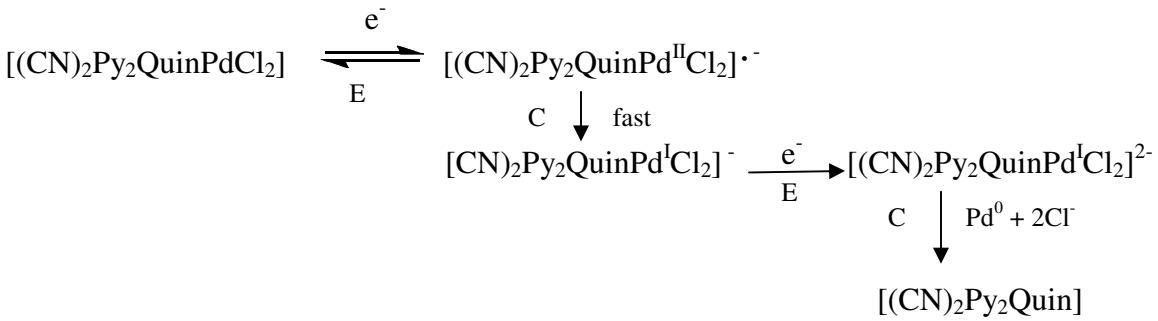

Scheme 4.2. Proposed ECEC Mechanism for Reduction of $[(CN)_2Py_2QuinPdCl_2]$.

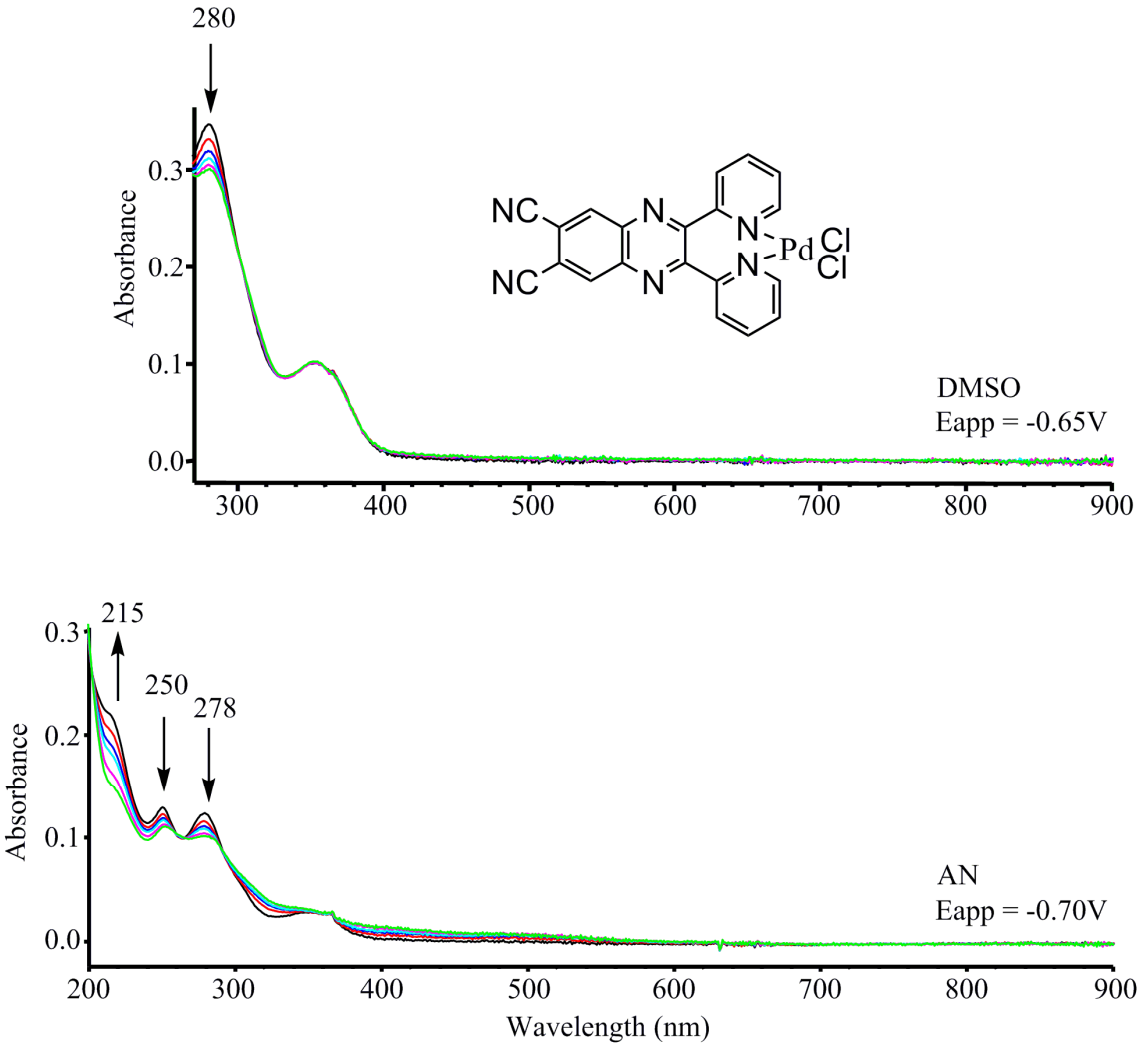

Figure 4.8: Spectral changes of the first reduction of $[(CN)_2Py_2QuinPdCl_2]$ in DMSO and AN, containing 0.2M TBAP.

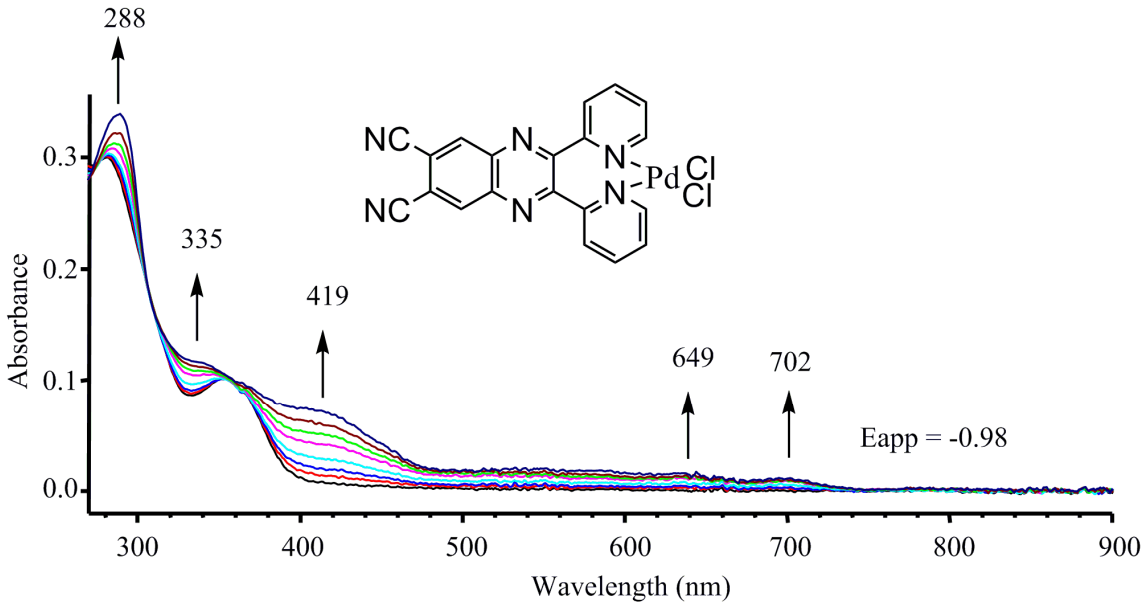

Figure 4.9: UV-visible spectral changes during controlled potential reduction of $[(CN)_2Py_2QuinPdCl_2]$ at -0.98 V in DMSO, containing 0.2M TBAP.

new absorption peaks. Similar changes are seen in AN (Figure 4.8) with a decrease in absorption at 278 nm and 250 nm, which could not be observed in DMSO, and the formation of a new peak at 215 nm. For the first reduction of $[(CN)_2Py_2PyzPdCl_2]$, Cai et al[1] showed that in pyridine there is a decrease in the only observable absorption at 309 nm, which corresponds with what is observed for its quinoxaline analogue.

4.2.3 Electronic Spectra and Related DFT/TDDFT Studies.

As mentioned earlier in this chapter, the UV-visible spectral changes previously observed upon the one-electron reduction of the neutral species in Chart 4.1 are characterized by a general bathochromic shift of the bands in the region 250-450 nm and by the appearance of new absorptions in the long wavelength region of the spectrum (500-900 nm). To our knowledge, these type of findings have no counterpart in the literature, the explanation apparently mainly residing on the fact that no electrochemical studies with analysis of the concomitant UV-visible spectral changes were reported for the formation of -1 charged species on the many compounds carrying dipyridino-, dithienyl- and diphenylpyrazine moieties either as such or as metal derivatives.[12-14, 19-28]

As detailed below, the results of our theoretical calculations will be presented and discussed as to the spin-density distribution for the monoanions of the unmetalated and metalated compounds and the electron affinity of the neutral and anionic species. Besides, the experimental UV-vis/near-IR spectral data are combined with theoretical calculations in an attempt to interpret the observed changes which occur upon one-electron reduction of the compounds of Charts 4.1.

In a good approximation, it can be said that the structural features of the neutral

unmetalated compounds [$(CN)_2Py_2Pyz$] and [$(CN)_2Py_2Quin$] species (Chart 4.1) in the gas phase, as found in the theoretical calculations, will closely approach those already known in the solid state by X-ray studies,[15, 29] which show the dicyanopyrazine and dicyanoquinoxaline fragments to be in an essentially planar arrangement, with the two pyridine rings positioned out of the plane of the pyrazine ring, forming dihedral angles within the range 35-45 degrees and pointing towards opposite directions. Previous theoretical studies in the gas phase for the compound [$(CN)_2Th_2Pyz$] indicate that the thienyl rings reside out of plane of the dicyanopyrazine fragment, orientation being such that the S atoms point in the same direction.[4] The geometric optimizations of the monoanions show that the addition of one electron, leading to [$(CN)_2Py_2Pyz]^{1-}$, [$(CN)_2Py_2Quin]^{1-}$ and [$(CN)_2Th_2Pyz]^{1-}$, slightly perturbs the overall geometry of the compounds. Figure 4.10A,C,E shows the structures of these anions, along with the (unrestricted SCF) spin density, highlighted in magenta to pictorially localize the excess electron. Since the spin density roughly resembles the SOMO (Singly Occupied Molecular Orbital), it can be seen that the added electron is mainly distributed on the benzopyrazine fragment in [$(CN)_2Py_2Quin]^{1-}$ and on the dicyanopyrazine moiety in [$(CN)_2Py_2Pyz]^{1-}$. Interestingly, it appears that the spin density in the reduced thienyl species [$(CN)_2Th_2Pyz]^{1-}$ pervades the dicyanopyrazine moiety and is extended to one of the two thienyl rings which is arranged nearly coplanar with the pyrazine ring. This coplanar positioning of the pyrazine ring with one thienyl ring was earlier observed by X-ray studies of unreduced [$(CN)_2Th_2Pyz$] in the solid state.[4]

For the metalated compounds [$(CN)_2Py_2QuinPtCl_2$] and [$(CN)_2Py_2PyzPtCl_2$], of

known structure (the present chapter and ref. 1 respectively), in which a rigid orientation of the pyridine rings is present due to coordination of the metal center, the excess electron spin density is shown to reside mainly on the conjugated π-system of the benzopyrazine and dicyanopyrazine fragments, respectively, its distribution resembling essentially that present in the corresponding unmetalated species.

Calculation of the energy difference between the anions and the corresponding neutral species allows one to easily compute the gas phase electron affinity (EA). In the case of the quinoxaline derivatives, the calculated gas phase EA values are 2.05, 2.74 and 2.78 eV for $[(CN)_2Py_2Quin]$, $[(CN)_2Py_2QuinPtCl_2]$ and $[(CN)_2Py_2QuinPdCl_2]$, respectively. Similarly, the EA values of the pyrazine derivatives $[(CN)_2Py_2Pyz]$ and $[(CN)_2Py_2PyzPtCl_2]$ are 1.93 and 2.68 eV, respectively. The half-wave reduction potential ($E_{1/2}$) is related to the gas phase EA through the following equation[28]

$$E_{1/2} = EA - \Delta\left(\Delta G_{solv}\right) + E_{SCE} \qquad (4.5)$$

where E_{SCE} is a negative constant and the second term of equation 4.5 is a contribution that comes from a difference of solvation energies, a term which remains roughly constant for structurally similar compounds. Since EA of the metalated compounds is ~0.7-0.8 eV larger than for the umetalated ones, within the hypothesis that the difference in solvation energies are smaller than that, we conclude that the reduction of $E_{1/2}$ upon metalation is mainly due to an increase of the in-vacuo EA. Therefore, we can attribute the reduction in $E_{1/2}$ to the presence of the electron withdrawing metallic groups, a situation which is consistent with what was pointed out by the electrochemical data described in the previous pages.

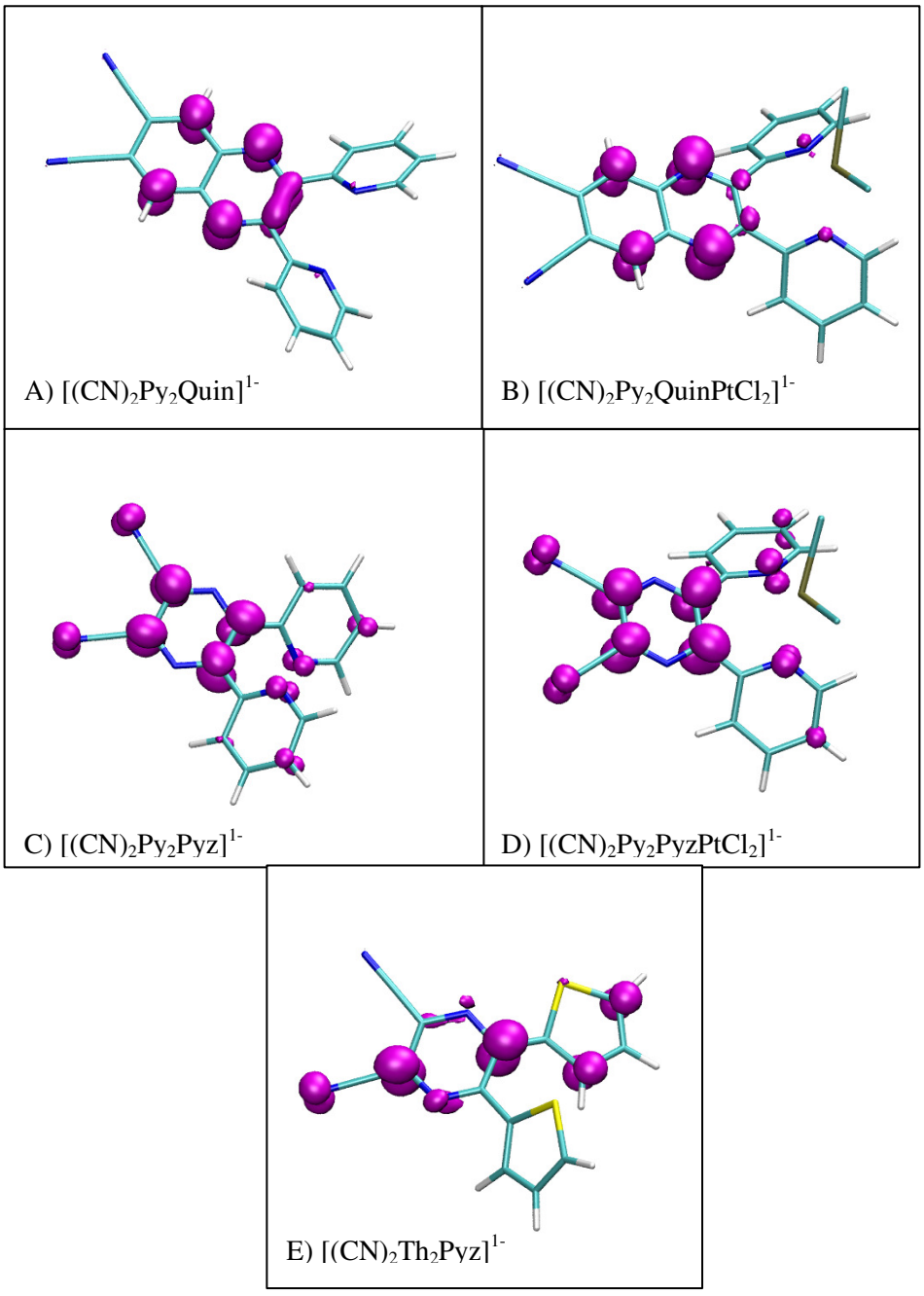

Figure 4.10. Illustration of spin density distribution, based on DFT studies, of the excess electron in the monoanions A) $[(CN)_2Py_2Quin]^{1-}$, B) $[(CN)_2Py_2QuinPtCl_2]^{1-}$, C) $[(CN)_2Py_2Pyz]^{1-}$, D) $[(CN)_2Py_2PyzPtCl_2]^{1-}$ and E) $[(CN)_2Th_2Pyz]^{1-}$.

4.2.4 UV-visible Spectral Behavior. Comparison of Experimental and Theoretical Findings.

Quantitative UV-Visible spectral data for the neutral and -1 charged unmetalated and metalated quinoxaline and pyrazine species and unmetalated thienyl and phenyl analogs are summarized in Table 4.3. The theoretical "stick" spectra along with the experimental UV-visible spectral selected calculated absorption wavelengths are reported in Table 4.4.

As can be seen in Figure 4.11, the fit between the experimental and theoretical results is excellent for the unmetalated species (A, C, E, F) and also satisfactory for the two platinated quinoxaline (B) and pyrazine species (D) in terms of the observed agreement between the profile of the absorption spectra and the sticks from theoretical calculations for both the unreduced (black) and reduced species (red). In general, the neutral molecules exhibit spectra with absorptions in the 250-400 nm region that are dominated by electronic transitions between the frontier orbitals. The involved Kohn and Sham orbitals have a strong π character, although account should be taken that our classification of the orbitals as π and π^* is purely qualitative since both the quinoxaline and pyrazine compounds are not rigidly planar. Upon reduction, the neutral species acquire an excess electron and their UV-Vis absorption spectra are characterized by low-energy absorption bands appearing in the region 500-900 nm and a general bathochromic shift of the high-lying bands is observed.

Focusing on the quinoxaline compounds, a scheme of the orbitals for the unmetalated species and observed changes upon one-electron reduction (spectra in Figure

4.11A) is reported in Figure 4.12A, where the energy level scheme of the Kohn and Sham orbitals of the neutral compound [$(CN)_2Py_2Quin$] are reported on the left and their counterparts for its anion [$(CN)_2Py_2Quin]^{1-}$ on the right. The orbitals for the anion are split onto the α and β sets since they come from an unrestricted reference. Summarily, qualitatively similar energy level diagrams are obtained for the other 0/-1 charged species (spectra in Figure 4.11 C,E,F).

The HOMO orbital for the neutral quinoxaline species (Figure 4.12) is delocalized over the entire molecule, and substantially made by a combination of the π system of the dicyanoquinoxaline fragment, with the two distinct π systems on the two pyridines. The LUMO is mainly π* in character and localized only on the dicyanoquinoxaline fragment. As to the energy level scheme of the related monoanion (Figure 4.12 on the right), a single orbital in the α set (SOMO) is partially filled with the excess electron. Its shape and symmetry closely resembles the LUMO of the neutral molecule, since it is not delocalized over the entire molecule, but is rather localized on the dicyanoquinoxaline portion of it, somewhat approaching the spin density shown in Figure 6A. Besides, the HOMO of the neutral compound, upon reduction, "splits" into the SOMO-1 of the anion in the α set and the HOMO-1 of the β set. The HOMO of the β set has a strong π character and is localized only on the dicyanoquinoxaline moiety. As it is shown in Table 4.4, which summarizes most of the UV-visible absorption bands detected in the 250-400 nm region for the present neutral molecules (3^{rd} and 4^{th} columns), related transitions are due to electronic excitations between the very first frontier orbitals.

As already pointed out, the spectra of the quinoxaline monoanion as well as those

Table 4.3. UV-Visible Spectral Data in DMSO, 0.1 M TBAP of various quinoxaline and pyrazine derivatives before and after first one electron reduction.

Compound	Solvent	λ_{max}, nm (logε)								Ref[a]
		Neutral		After 1st reduction						
$[(CN)_2Py_2Quin]$	DMSO	284 (4.52)	355 (4.03)	277 (4.56)	337 (4.33)	420 (3.83)	585 (3.75)	641 (3.83)	700 (3.73)	tw
$[(CN)_2Py_2QuinPdCl_2]$	DMSO	280 (4.04)	355 (3.59)	288 (4.04)		416 (3.37)			700 (2.58)	tw
$[(CN)_2Py_2QuinPtCl_2]$	DMSO	279 (4.38)	377 (3.62)	277 (4.32)	332 (3.96)	415 (3.42)		646 (3.34)		tw
$[(CN)_2Py_2Pyz]$	DMSO	314 (5.15)		314 (4.95)		390 (5.12)		610(4.90)		1
	Pyridine	320 (5.11)		323 (4.97)		395 (5.09)		621(4.86)		1
$[(CN)_2Py_2PyzPdCl_2]$	DMSO	306 (5.16)		306 (4.94)		395 (5.09)		612(4.87))		tw
$[(CN)_2Py_2PyzPtCl_2]$	DMSO	300 (4.96)		397 (4.91)					710 (4.83)	tw
$[(CN)_2Th_2Pyz]$	DMSO	310 (4.20)	383 (4.25)	304 (4.18)		398 (4.08)		640 (3.36)		tw
	Pyridine	317 (4.60)	390 (4.75)	317 (4.53)		402 (4.63)		623 (4.07)		1
$[(CN)_2Ph_2Pyz]$	DMSO	336 (3.76)		338 (3.66)		389 (3.37)	497 (3.13)	602 (2.70)	776 (2.60)	tw
	Pyridine	340 (4.83)		340 (4.66)		389 (4.77)	503	621 (4.30)	798	1

[a]tw = this work

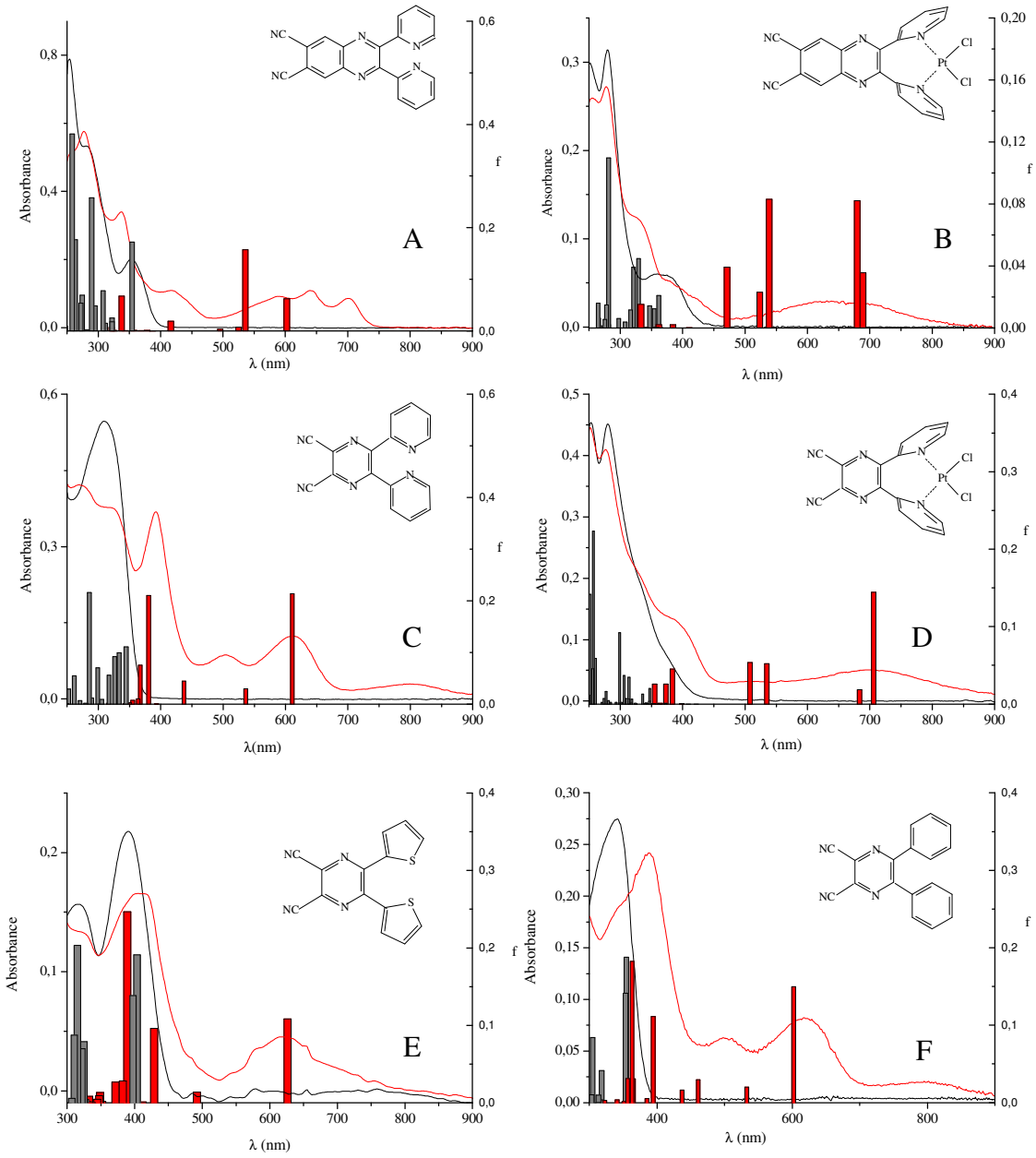

Figure 4.11. Experimental UV-visible spectra of neutral (black) and one-electron reduced (red) quinoxaline and pyrazine derivatives. A, B, C, D,: spectra in DMSO; E, F: spectra in pyridine. Sticks are from theoretical calculations. On the left scale there is the measured absorbance and the oscillator strength from TDDFT calculations is on the right scale.

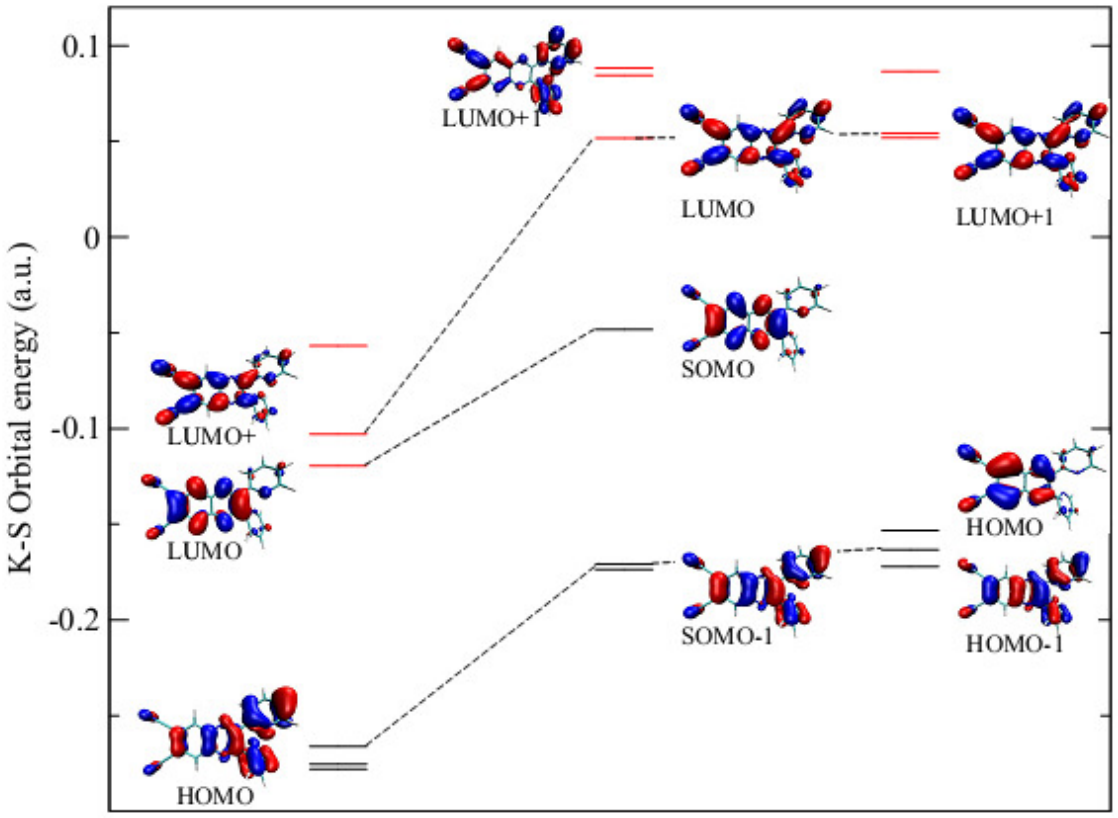

Figure 4.12: Kohn-Sham energy levels for neutral $[(CN)_2Py_2Quin]$ (left) and $[(CN)_2Py_2Quin]^{1-}$ (right). Occupied orbitals are in black and virtual ones are in red. For each compound we report the energy of the HOMO-2, HOMO-1, HOMO, LUMO, LUMO+1 and LUMO+2. Some of the relevant orbitals are also sketched. The orbitals of the anion are divided in 2 sets, one for each spin projection of the electron. The correlation between the orbitals of the neutral and the anion (indicated by the dashed lines) is purely qualitative and based only on consideration of symmetry and shape.

of the other studied analogs (red curves in Figure 4.11C,E,F), exhibit absorptions in the region 500-900 nm as an exclusive feature of these anionic species. Using as reference the orbital scheme in Figure 4.12 and the outcomes of the TDDFT calculations, it can be shown that these low-energy absorption bands, are mainly due to single electronic excitations from the (α) SOMO to the (α) LUMO+1 orbital. In addition, all the anions present a very weak absorption due to a (α) SOMO → (α) LUMO excitation that can be seen above 1500 nm outside the experimental range of observations. At higher energies, the excitation patterns leading to intense absorption bands arising at 250-400 nm in the anions are more complex in nature and are due to many simultaneous single electron transitions which also involve the β orbital. In particular the transitions originating from the HOMO and HOMO-1 orbitals of the β-set are mainly responsible for these absorption lines.

With reference to the metalated neutral compounds, their orbital schemes appear substantially different from those of the related unmetalated species because of the presence of the orbitals of the metal containing unit. In fact, the HOMO orbital is generally localized on the metal-chloride unit and is made by a combination of a *d* orbital of the metal and two *p* orbitals on the chlorine atoms. The energetic levels of the Kohn Sham orbitals of the quinoxaline platinated derivative [$(CN)_2Py_2QuinPtCl_2$] are depicted in Figure 4.13 (right) together with those of the unmetalated derivative (left). It can be seen that, upon metalation (left → right), the orbitalic scheme is completely altered due to the presence of the orbitals of the $PtCl_2$ unit in the metalated species. Since there is no direct covalent bonding between the $PtCl_2$ unit and the rest of the molecule, the resulting

Table 4.4: TDDFT selected absorption wavelengths (nm) for compounds A, B, C, D, E and F. It is also indicated the corresponding largest weight 1-electron single excitation. H stands for HOMO, L for LUMO and S for SOMO.

Compound		*λ (Neutral)*		*λ (Anion)*	
$[(CN)_2Py_2Quin]$	A	362	H → L	607	αS → αL+1
		298	H-2 → L+1	541	αS → αL+6
		272	H-7 → L	423	αS → αL+7
		268	H-5 → L+1	346	βH → βL+1
$[(CN)_2Py_2QuinPtCl_2]$	B	370	H-1 → L	679	αS → αL+1
		338	H-11 → L	540	αS → αL+3
		330	H-4 → L	483	αS → αL+7
		290	H-5 → L	383	βH-3 → βL+1
$[(CN)_2Py_2Pyz]$	C	344	H → L	610	αS → αL+1
		333	H → L+1	536	αS → αL+3
		326	H-1 → L+1	437	αS → αL+7
		285	H-3 → L	380	βH → βL
$[(CN)_2Py_2PyzPtCl_2]$	D	299	H-1 → L+1	705	αS → αL+1
		256	H-5 → L+1	534	αS → αL+3

Table 4.4 cont. TDDFT selected absorption wavelengths (nm) for compounds A, B, C, D, E and F. It is also indicated the corresponding largest weight 1-electron single excitation. H stands for HOMO, L for LUMO and S for SOMO.

Compound		*λ (Neutral)*		*λ (Anion)*	
$[(CN)_2Py_2PyzPtCl_2]$		251	H-5 → L	508	αS → αL+4
				383	βH-1 → βL
$[(CN)_2Th_2Pyz]$	E	403	H → L	626	αS → αL+1
		397	H-1 → L+1	428	αS-1 → αL+1
		315	H-1 → L+2	389	βH → βL+1
$[(CN)_2Ph_2Pyz]$	F	354	H → L	602	αS → αL+1
		353	H → L+1	533	αS → αL+2
		282	H-2 → L	394	βH → βL
				363	βH → βL+1

orbital set can be roughly seen as a superposition of the non metalated scheme on the left and the $PtCl_2$ energetic levels. The presence of the $PtCl_2$ unit causes a decrease in energy of the π orbitals localized over the conjugated molecule, whereas the HOMO and the orbitals immediately below in energy are now completely localized on the $PtCl_2$ unit (as an example the HOMO and HOMO-2 are shown in Figure 4.13). The electronic excitation in the platinated species is rather complex since it now involves simultaneous excitations of the electrons on the $PtCl_2$ unit and on the quinoxaline moiety. Again referring to Figure 4.13, the HOMO $\rightarrow$ LUMO transition has a near zero oscillator strength due to the fact that the involved orbitals have a very small superposition. The intense transitions that can be seen on the neutral metalated molecules involve a rather complicated excitation schemes which include excitations coming from low-lying π orbitals (such as the HOMO-5 in Figure 4.13) and from the orbitals localized on the $PtCl_2$ unit (such as the HOMO-2 in Figure 4.13) to the LUMO π^* that remains localized over the quinoxaline moiety. Moreover, it can be noticed here that the available spectral data (Table 4.3, Figure 4.11C,D) and achieved information from theoretical calculations (Table 4.4, Figure 4.14) for $[(CN)_2Py_2Pyz]$, its platinated derivative $[(CN)_2Py_2PyzPtCl_2]$ and their corresponding -1 species suggest a profile of discussion quite similar to that already presented for the quinoxaline compounds and hence are not further considered. As detailed in Table 4.4, in the non metalated neutral compounds (Figure 4.11A,C,E,F) the excitation scheme is rather simple and the observed transitions sequence begins with a HOMO $\rightarrow$ LUMO excitation and continues by mixing higher energy excitations between the very first frontiers orbitals. A typical recurring pattern is easily discernible

also in their respective reduced forms where the transitions at low energies are due to excitations in the α set from the SOMO to the LUMO+1 and adjacent orbitals while those at high energy involve, instead, the HOMO, LUMO and adjacent orbitals of the β set. As discussed above, metalation produces relevant changes in the orbital energy pattern making the electronic spectra more difficult to interpret and assign. Even in these cases, however, the spectral features between 600 and 700 nm in the reduced molecules are still given by a SOMO → LUMO+1 electronic excitation.

4.3 Conclusions.

UV-visible spectral and electrochemical results in solution of nonaqueous solvents (DMSO, CH_3CN, or pyridine) made available on a series of previously studied dicyanopyrazine compounds carrying vicinal pyridine, thienyl or phenyl rings, i.e., 2,3-dicyano-5,6-di(2-pyridyl)-1,4-pyrazine, [$(CN)_2Py_2Pyz$], 2,3-dicyano-5,6-di(2-thienyl)-1,4-pyrazine, [$(CN)_2Th_2Pyz$] and 2,3-dicyano-5,6-diphenyl-1,4-pyrazine, [$(CN)_2Ph_2Pyz$], and the metal derivatives [$(CN)_2Py_2PyzMCl_2$] (M = Pd^{II}, Pt^{II}) have been added to parallel similar information on the dicyanoquinoxaline compound 2,3-di(2-pyridyl)-6,7-dicyano-1,4-quinoxaline, [$(CN)_2Py_2Quin$] and its metal derivatives [$(CN)_2Py_2QuinMCl_2$] (M = Pd^{II}, Pt^{II}). As was the case for the [$(CN)_2Py_2Pyz$] and the related metalated species, it is confirmed that definitely more facile first and second reductions take place (by 250-300 mV vs SCE) for the quinoxaline compounds once [$(CN)_2Py_2Quin$] is changed to its $PtCl_2$ and $PdCl_2$ complexes, due to the electron withdrawing effects of the metal centers. It has been established that the first one-electron uptake for the majority of compounds (made exception for the Pd^{II} species)

leads reversibly to the formation of the -1 charged species. This is accompanied by changes of the UV-visible spectra in the entire region 300-900 nm consisting of a systematic bathochromic shift of the absorptions in the region 300-450 nm coupled with the appearance of new intense absorptions in the lower energy region (500-900 nm). TDDFT calculations establish that the spin density of the excess electron in the -1 charged species of the unmetalated compounds is exclusively on the benzopyrazine moiety in the quinoxaline species $[(CN)_2Py_2Quin]^{1-}$, mainly located on the dicyanopyrazine fragment for $[(CN)_2Py_2Pyz]^{1-}$, and expands through the NC-Pyz-Thienyl axis for the reduced thienyl species $[(CN)_2Th_2Pyz]^{1-}$. Single excitations between the Kohn-Sham orbitals, lead to quite a satisfactory interpretation of the observed UV-visible spectral features which typically characterize the neutral and -1 reduced species. In particular, the new absorptions in the near-IR region for the -1 charged species are assigned to transitions from the SOMO (singly occupied molecular orbital) to the LUMO +1 energy level (see Figures 4.12 and 4.13), certainly a result of relevant significance of the present attempted fitting between experimental and theoretical calculations.

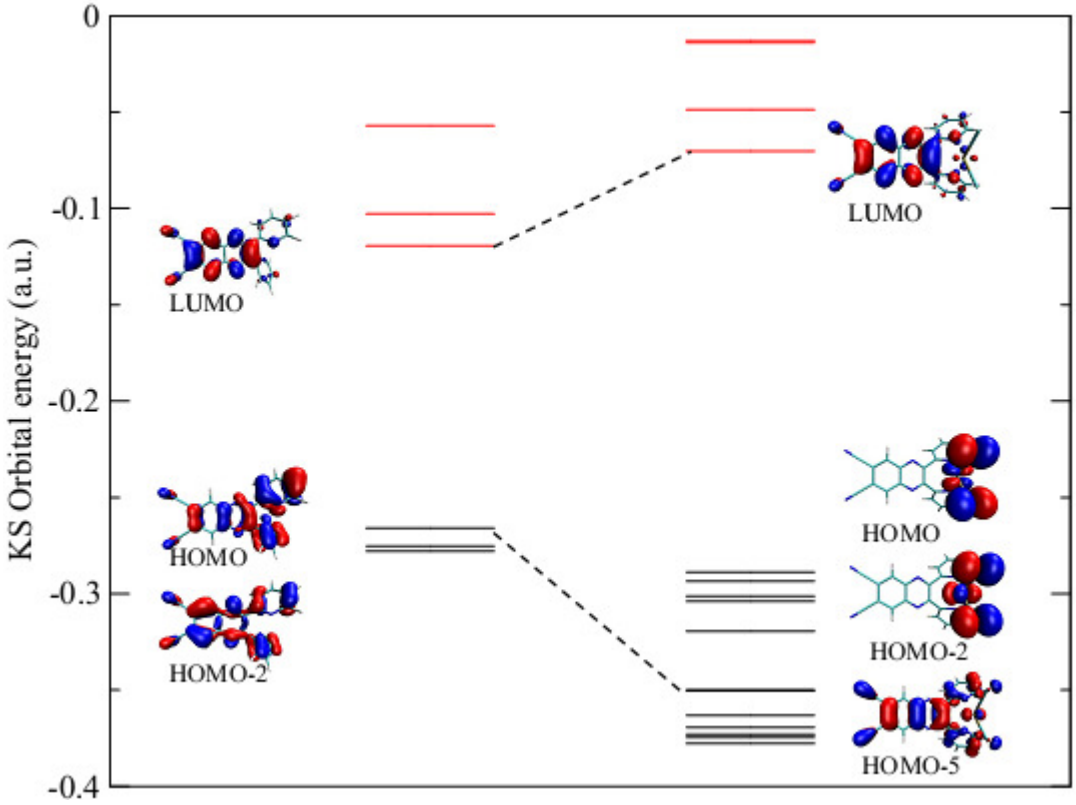

Figure 4.13: Kohn-Sham energy levels for $[(CN)_2Py_2Quin]$ (left) and platinated $[(CN)_2Py_2QuinPtCl_2]$ (right). Occupied orbitals are in black and virtual ones are in red. For each compound we report the energy only of the frontiers orbitals involved in the low-lying UV transitions. Some of the relevant orbitals are also sketched. The correlation between the sets of orbitals (indicated by the dashed lines) is purely qualitative and based only on consideration of symmetry and shape.

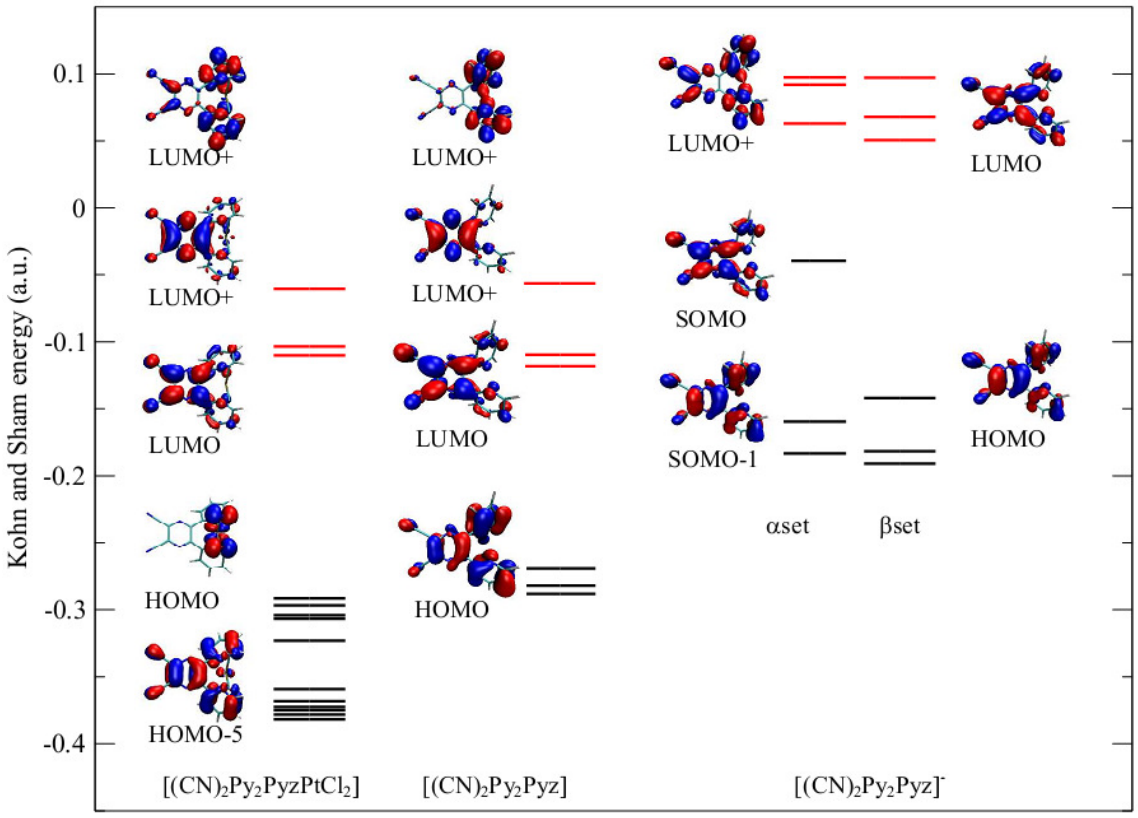

Figure 4.14: Kohn-Sham energy levels for $[(CN)_2Py_2Pyz]$ (middle), $[(CN)_2Py_2PyzPtCl_2]$ (left) and $[(CN)_2Py_2Pyz]^-$ (right).

4.4 References

1. Cai, X.; Donzello, M. P.; Viola, E.; Rizzoli, C.; Ercolani, C.; Kadish, K., *Inorg. Chem.* **2009,** ***48***, 7086.
2. Bergami, C.; Donzello, M. P.; Monacelli, F.; Ercolani, C.; Kadish, K. M., *Inorg. Chem.* **2005,** *44*, 9862-9873.
3. De Mori, G.; Fu, Z.; Viola, E.; Cai, X.; Ercolani, C.; Donzello, M. P.; Kadish, K. M., *Inorg. Chem.* **2011,** *50*, 8225.
4. Donzello, M. P.; De Mori, G.; Viola, E.; Ercolani, C.; Bodo, E.; Mannina, L.; Capitani, D.; Rizzoli, C.; Gontrani, L.; Aquilanti, G.; Kadish, K. M.; D'Angelo, P., *Inorganic Chemistry* **2011,** *50*, 12116-12125.
5. Donzello, M. P.; Viola, E.; Bergami, C.; Dini, D.; Ercolani, C.; Giustini, M.; Kadish, K. M.; Meneghetti, M.; Monacelli, F.; Rosa, A.; Ricciardi, G., *Inorg. Chem.* **2008,** *47*, 8757-8766.
6. Donzello, M. P.; Viola, E.; Cai, X.; Mannina, L.; Ercolani, C.; Kadish, K. M., *Inorg. Chem.* **2010,** *49*, 2447-2456.
7. Donzello, M. P.; Viola, E.; Cai, X.; Mannina, L.; Rizzoli, C.; Ricciardi, G.; Ercolani, C.; Kadish, K.; Angela, R., *Inorg. Chem.* **2008,** *47*, 3903-3919.
8. Donzello, M. P.; Viola, E.; Ercolani, C.; Fu, Z.; Futur, D.; Kadish, K., *Inorg. Chem.* **2012,** *51*, 12548.
9. Donzello, M. P.; Viola, E.; Mannina, L.; Barteri, M.; Fu, Z.; Ercolani, C., *J. Porphyrins Phthalocyanines* **2011,** *15*, 984-994.

10. Manet, I.; Manoli, F.; Donzello, M. P.; Ercolani, C.; Vittori, D.; Cellai, L.; Monti, S., *Org. Biomol. Chem.* **2011,** *9*, 684-688.

11. Viola, E.; Donzello, M. P.; Ciattini, S.; Portalone, G.; Ercolani, C., *Eur. J. Inorg. Chem.* **2009**, 1600-1607.

12. Granifo, J.; Vargas, M. E.; Rocha, H.; Garland, M. T.; Baggio, R., *Inorg. Chim. Acta* **2001,** *321*, 209-214.

13. Granifo, J.; Vargas, M. E.; Garland, M. T.; Baggio, R., *Inorg. Chim. Acta* **2000,** *305*, 143-150.

14. Rubino, S.; Portanova, P.; Girasolo, A.; Calvaruso, G.; Orecchio, S.; Stocco, G. C., *Eur. J. Med. Chem.* **2009,** *44*, 1041-1048.

15. Haas, M.; Liu, S.; Neels, A.; Decurtins, S., *Eur. J. Org. Chem.* **2006,** *24*, 5467.

16. Donzello, M. P.; De Mori, G.; Futur, D.; Fu, Z.; Astolfi, M. L.; Rizzoli, C.; Ercolani, C.; Mannina, L.; Bodo, E.; Kadish, K., *Dalton Trans* **2013,** *submitted*.

17. Hirt, R. C.; King, F. T.; Cavagnol, J. C., *J. Chem. Phys.* **1956,** *25*, 574.

18. Halverson, F.; Hirt, R. C., *J. Chem. Phys.* **1951,** *19*, 711.

19. Bandoli, G.; Gerber, T. I. A.; Jacobs, R.; du Preez, J. G. H., *Inorganic Chemistry* **1994,** *33*, 178-9.

20. Chesnut, D. J.; Kusnetzow, A.; Birge, R. R.; Zubieta, J., *Inorganic Chemistry* **1999,** *38*, 2663-2671.

21. Escuer, A.; Comas, T.; Ribas, J.; Vicente, R.; Solans, X.; Zanchini, C.; Gatteschi, D., *Inorg. Chim. Acta* **1989,** *162*, 97-103.

22. Escuer, A.; Vicente, R.; Comas, T.; Ribas, J.; Gomez, M.; Solans, X., *Inorg. Chim. Acta* **1990,** *177*, 161-6.

23. Escuer, A.; Vicente, R.; Comas, T.; Ribas, J.; Gomez, M.; Solans, X.; Gatteschi, D.; Zanchini, C., *Inorg. Chim. Acta* **1991,** *181*, 51-60.

24. Gordon, K. C.; Al-Obaidi, A. H. R.; Jayaweera, P. M.; McGarvey, J. J.; Malone, J. F.; Bell, S. E. J., *J. Chem. Soc., Dalton Trans.* **1996**, 1591-6.

25. Nicolo, F.; Cusumano, M.; Di Pietro, M. L.; Scopelliti, R.; Bruno, G., *Acta Crystallogr., Sect. C: Cryst. Struct. Commun.* **1998,** *C54*, 485-487.

26. Rarig, R. S., Jr.; Hagrman, P. J.; Zubieta, J., *Solid State Sci.* **2002,** *4*, 77-82.

27. Rillema, D. P.; Taghdiri, D. G.; Jones, D. S.; Worl, L. A.; Meyer, T. J.; Levy, H. A.; Keller, C. D., *Inorganic Chemistry* **1987,** *26*, 578-85.

28. Ruoff, R. S.; Kadish, K. M.; Boulas, P.; Chen, E. C. M., *J. Phys. Chem.* **1995,** *99*, 8843.

29. Donzello, M. P.; Ou, Z.; Monacelli, F.; Ricciardi, G.; Rizzoli, C.; Ercolani, C.; Kadish, K. M., *Inorg. Chem.* **2004,** *43*, 8626.